

# Composition and Alignment of Diffusion Models using Constrained Learning

Shervin Khalafi Ignacio Hounie Dongsheng Ding Alejandro Ribeiro

## Abstract

Diffusion models have become prevalent in generative modeling due to their ability to sample from complex distributions. To improve the quality of generated samples and their compliance with user requirements, two commonly used methods are: (i) Alignment, which involves fine-tuning a diffusion model to align it with a reward; and (ii) Composition, which combines several pre-trained diffusion models, each emphasizing a desirable attribute in the generated outputs. However, trade-offs often arise when optimizing for multiple rewards or combining multiple models, as they can often represent competing properties. Existing methods cannot guarantee that the resulting model faithfully generates samples with all the desired properties. To address this gap, we propose a constrained optimization framework that unifies alignment and composition of diffusion models by enforcing that the aligned model satisfies reward constraints and/or remains close to (potentially multiple) pre-trained models. We provide a theoretical characterization of the solutions to the constrained alignment and composition problems and develop a Lagrangian-based primal-dual training algorithm to approximate these solutions. Empirically, we demonstrate the effectiveness and merits of our proposed approach in image generation, applying it to alignment and composition, and show that our aligned or composed model satisfies constraints effectively, and improves on the equally-weighted approach. Our implementation can be found at [https://github.com/shervinkhalafi/constrained\\_comp\\_align](https://github.com/shervinkhalafi/constrained_comp_align). <sup>1</sup>

## 1 Introduction

Diffusion models have emerged as the tool of choice for generative modeling in a variety of settings [36, 3, 48, 9], image generation being most prominent among them [35]. Users of these diffusion models would like to adapt them to their specific preferences, but this aspiration is hindered by the often enormous cost and complexity of their training [46, 54]. For this reason, *alignment* and *composition* of what, in this context, become *pretrained* models, has become popular [28, 29].

Regardless of whether the goal is alignment or composition, we want to balance what are most likely conflicting requirements. In alignment tasks, we want to stay close to the pretrained model while deviating sufficiently so as to affect some rewards of interest [16, 13]. In composition tasks we are given several pretrained models and our goal is to sample from their union or intersection [14, 1]. The standard approach to balance these requirements involves the use of weighted averages. This can be a linear

<sup>\*</sup>S. Khalafi, I. Hounie, D. Ding, and A. Ribeiro are with the University of Pennsylvania, Philadelphia, PA 19104. E-mails: {shervink, ihounie, dongshed, aribeiro}@seas.upenn.edu

<sup>1</sup>Direct questions regarding implementation to shervink@seas.upenn.edu.

combination of score functions in composition problems [14, 1] or may involve optimizing a loss given by a linear combination of a Kullback-Leibler (KL) divergence and a reward [16] in the case of alignment.

In this work, we propose a unified view of alignment and composition via the lens of constrained learning [7, 6]. As their names indicate, constrained alignment and constrained composition problems balance conflicting requirements using constraints instead of weights. Learning with constraints and learning with weights are related problems – indeed, we will train constrained diffusion models in their Lagrangian forms. Yet, they are also fundamentally different. In our constrained formulation, the constraint thresholds that need to be satisfied are the design parameters of interest. Tuning these thresholds is more interpretable than tuning the weights of regularizers added to a training objective. In many cases, such as the constrained composition formulation, this hyperparameter tuning can even be avoided entirely. These advantages are particularly evident in problems with multiple constraints as discussed in Sections 3 and 4. We next outline our key contributions in alignment and composition.

**Alignment.** For alignment, we formulate a reverse KL divergence-constrained optimization problem that minimizes the reverse KL divergence to a pre-trained model, subject to expected reward constraints. The threshold for each reward constraint can be user-specified or automatically selected using a heuristic approach explained in Section 5. In Section 3 we show that the solution of this alignment problem is the pretrained model distribution scaled by an exponential function of a weighted sum of reward functions . To solve this problem with diffusion models, we establish strong duality, which enables us to employ a Lagrangian dual-based approach to develop a primal-dual training algorithm.

We demonstrate the differences between constrained and weighted alignment in computational experiments in Section 5.1. The constrained approach easily scales to fine-tuning with multiple rewards, while avoiding the need for extensive hyperparameter search to find suitable weights. Moreover, specifying reward thresholds is more intuitive than selecting weights for each regularizer. Furthermore, without constraints, it is easy to overfit to one or multiple of the rewards and completely diverge from the pretrained model. In contrast, our method finds the closest model to the pretrained one that satisfies the reward constraints as seen in Figure 4.

**Composition.** For composition of multiple models, we propose using KL divergence constraints to ensure the closeness to each individual model. It is important to distinguish composition with *reverse* KL and *forward* KL constraints. As shown in [21], using forward KL constraints results in the composed model sampling from a weighted mixture of the individual distributions. In the main paper we focus on composition with reverse KL constraints, while we discuss forward KL constraints in Appendix D. In Section 4, we characterize the solution of the constrained optimization problem with *reverse* KL divergence constraints as a tilted product of the individual distributions. To solve this problem with diffusion models, we similarly establish strong duality and develop a primal-dual training algorithm.

We demonstrate properties of constrained composition of models in computational experiments in Section 5.2. We observe that if the composition weights are not chosen properly, it can lead to the composed model being biased towards some of the individual models while ignoring others. Constrained composition helps avoid this by finding optimal weights that ensure closeness to each individual distribution. When composing multiple text-to-image models each finetuned on a different reward function, using constraints leads to optimal weights that result in the composed model having better performance on all of the rewards compared to just composing them with equal weights.

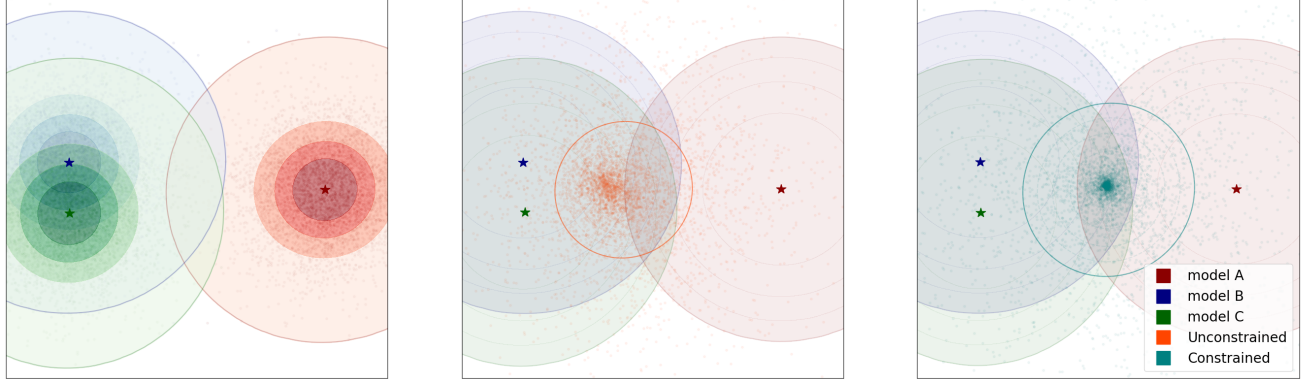


Figure 1: Product composition (AND): (left) Three Gaussian distributions being composed. (middle) Composition using equal weights and (right) with constraints. The constrained model samples from the intersection of the three models.

## 2 Composition and Alignment in Distribution Space

**Reward alignment:** Given a pretrained model  $q$  and a set of  $m$  rewards  $\{r_i(x)\}_{i=1}^m$  that can be evaluated on a sample  $x$ , we consider the *reverse* KL divergence  $D_{\text{KL}}(p \parallel q) := \int p(x) \log(p(x)/q(x))dx$  that measures the difference between a distribution  $p$  and the pretrained model  $q$ . Additionally, for each reward  $r_i$ , we define a constant  $b_i$  standing for requirement for reward  $r_i$ . We formulate a constrained alignment problem that minimizes a reverse KL divergence subject to  $m$  constraints,

$$p^* = \underset{p}{\operatorname{argmin}} \ D_{\text{KL}}(p \parallel q) \quad \text{subject to } \mathbb{E}_{x \sim p}[r_i(x)] \geq b_i \text{ for } i = 1, \dots, m. \quad (\text{UR-A})$$

As per (UR-A), the constrained alignment problem is solved by the distribution  $p^*$  that is closest to the pretrained one  $q$  as measured by the reverse KL divergence  $D_{\text{KL}}(p \parallel q)$  among those whose expected rewards  $\mathbb{E}_{x \sim p}[r_i(x)]$  accumulate to at least  $b_i$ . By ‘pretrained model’, we refer to the underlying distribution of the samples generated by the pretrained model. Let the primal value  $P_{\text{ALI}}^* := D_{\text{KL}}(p^* \parallel q)$ .

**Product composition (AND):** Given a set of  $m$  pretrained models  $\{q_i\}_{i=1}^m$ , we formulate a constrained composition problem that solves a reverse KL-constrained optimization problem,

$$(p^*, u^*) = \underset{p, u}{\operatorname{argmin}} \ u \quad \text{subject to } D_{\text{KL}}(p \parallel q_i) \leq u \text{ for } i = 1, \dots, m. \quad (\text{UR-C})$$

In (UR-C), the decision variable  $u$  is an upper bound on  $m$  KL divergences between a distribution  $p$  and  $m$  pretrained models  $\{q_i\}_{i=1}^m$ . Partial minimization over  $u$  allows us to search for a distribution  $p$  that minimizes a common upper bound. Thus, the optimal solution  $p^*$  minimizes the maximum KL divergence among  $m$  terms, each computed between  $p$  and a pretrained model. The epigraph formulation (UR-C) is useful in practice, as the constraint threshold  $u$  is updated dynamically during training. Let the primal value be  $P_{\text{AND}}^* := u^*$ . See Figure 1 for an illustration. The unconstrained model composed with equal weights is biased towards the distributions that are closer to each other.

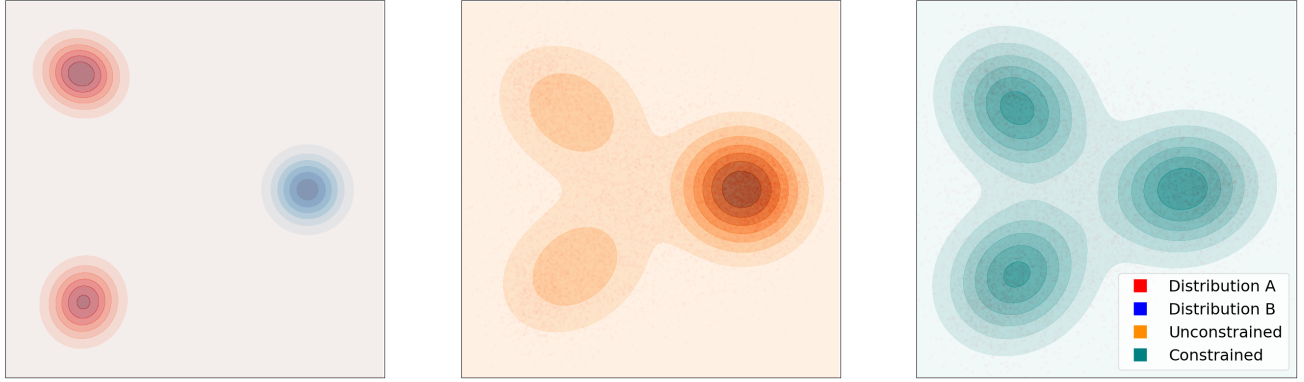


Figure 2: Mixture composition (OR): (left) Two of Gaussian mixtures being composed. One has two modes and the other has only a single mode. (middle) Composition using equal weights and (right) with constraints.

**Mixture composition (OR):** A different composition modality that also fits within our constrained framework is the *forward* KL-constrained composition problem. We obtain this formulation by replacing the *reverse* divergence  $D_{\text{KL}}(p \parallel q_i)$  in (UR-C) with the *forward* KL divergence  $D_{\text{KL}}(q_i \parallel p)$ ,

$$(p^*, u^*) = \underset{p, u}{\operatorname{argmin}} \quad \text{subject to } D_{\text{KL}}(q_i \parallel p) \leq u \text{ for } i = 1, \dots, m. \quad (\text{UF-C})$$

We note that mixture composition has been studied in a related but slightly different constrained setting in [21]. There, it is shown that the solution of the constrained problem (UF-C) learns to sample from each distribution proportional to its entropy. We verify this empirically as seen in Figure 2, where the constrained model learns to sample more often from the distribution with two modes that has a higher entropy in contrast to the equally weighted composition that samples equally from both distributions, leading to unbalanced sampling from the modes. Since the algorithm design and analysis for (UF-C) closely resemble those in [21], mixture composition is not the focus of this work. For completeness, we discuss and compare it with product composition in Appendix D.

The reverse KL-based composition (UR-C) tends to sample at the intersection of the pretrained models  $\{q_i\}_{i=1}^m$ , whereas the forward KL-based composition (UF-C) tends to sample at the union of the pretrained models  $\{q_i\}_{i=1}^m$ . Thus, product composition enforces a conjunction (logical AND) across pretrained models, while mixture composition corresponds to a disjunction (logical OR). This is closely related to the well-known mean-seeking and mode-seeking behaviors of forward and reverse KL, respectively. We stress that Problems (UR-A), (UR-C), and (UF-C) should be viewed as canonical formulations; the methods proposed in this paper can be readily adapted to solve their variants, e.g., mixture composition with reward constraints.

## 2.1 KL divergence for diffusion models

We provide an overview of diffusion models. A generative diffusion model consists of forward and backward processes. In the forward process, we add Gaussian noise  $\epsilon_t$  to a clean sample  $\bar{X}_0 \sim \bar{p}_0$  over  $T$

time steps,

$$\bar{X}_t = \sqrt{\frac{\alpha_t}{\alpha_{t-1}}} \bar{X}_{t-1} + \sqrt{1 - \frac{\alpha_t}{\alpha_{t-1}}} \epsilon_t, \quad \text{for } t \in \{1, \dots, T\} \quad (1)$$

where  $\epsilon_t \sim \mathcal{N}(0, I)$  and  $\{\alpha_t\}_{t=1}^T$  is a decreasing sequence of coefficients called the noise schedule. We denote the marginal density of  $\bar{X}_t$  at time  $t$  as  $\bar{p}_t(\cdot)$ . Given a  $d$ -dimensional score predictor function  $s(x, t)$ :  $\mathbb{R}^d \times \{1, \dots, T\} \rightarrow \mathbb{R}^d$ , we define a backward denoising diffusion implicit model (DDIM) process [40],

$$X_{t-1} = \sqrt{\frac{\alpha_{t-1}}{\alpha_t}} X_t + \gamma_t s(X_t, t) + \sigma_t \epsilon_t \quad (2)$$

where  $X_T \sim \mathcal{N}(0, I)$ ,  $\epsilon_t \sim \mathcal{N}(0, I)$ , and  $\{\sigma_t^2\}_{t=1}^T$  is the variance schedule determining the level of randomness in the backward process (e.g.,  $\sigma_t = 0$  leads to deterministic trajectories), and  $\gamma_t := \sqrt{\frac{\alpha_{t-1}}{\alpha_t}}(1 - \alpha_t) - \sqrt{(1 - \alpha_{t-1} - \sigma_t^2)(1 - \alpha_t)}$  is determined by the variance schedule  $\sigma_t$  and the noise schedule  $\alpha_t$ . Given the process (2) using a specific function  $s(x, t)$ , we denote the marginal density of  $X_t$  as  $p_t(\cdot; s)$  and the joint distribution over the entire process as  $p_{0:T}(x_{0:T}; s)$ .

In the score-matching formulation [41], a denoising score-matching objective is minimized to obtain a function  $s^*$  that approximates the true score function of the forward process, i.e.,  $s^*(x, t) \approx \nabla \log \bar{p}_t(x)$ . Then, the marginal densities of the backward process (2) match those of the forward process (1), i.e.,  $p_t(\cdot; s^*) = \bar{p}_t(\cdot)$  for all  $t$ . Thus, we can run the backward process to generate samples  $x_0 \sim p_0$  that resemble samples from the original data distribution  $\bar{x}_0 \sim \bar{p}_0$ .

We denote the KL divergence between two joint distributions  $p, q$  over the entire backward process by  $D_{\text{KL}}(p_{0:T}(\cdot) \parallel q_{0:T}(\cdot))$ , which is known as the path-wise KL divergence [16, 18]. This path-wise KL divergence is often used in alignment to quantify the gap between finetuned and pretrained models.

**Lemma 1** (Path-wise KL divergence). *If two backward processes  $p_{0:T}(\cdot)$  and  $q_{0:T}(\cdot)$  have the same variance schedule  $\sigma_t$  and noise schedule  $\alpha_t$ , then the reverse KL divergence between them is given by*

$$D_{\text{KL}}(p_{0:T}(\cdot; s_p) \parallel p_{0:T}(\cdot; s_q)) = \sum_{t=1}^T \mathbb{E}_{x_t \sim p_t(\cdot; s_p)} \left[ \frac{\gamma_t^2}{2\sigma_t^2} \|s_p(x_t, t) - s_q(x_t, t)\|^2 \right]. \quad (3)$$

See Appendix C.1 for proof. In the proof we also consider the relaxation of the same variance and noise schedule assumptions. While the path-wise KL divergence is a useful regularizer for alignment, when composing multiple models, the point-wise KL divergence  $D_{\text{KL}}(p_0(\cdot) \parallel q_0(\cdot))$  is a more natural measure of the closeness between two diffusion models. This is because we mainly care about the closeness of the final distributions of the samples:  $p_0(\cdot)$ ,  $q_0(\cdot)$ , and not the underlying processes:  $p_{0:T}(\cdot)$ ,  $q_{0:T}(\cdot)$ . In this work, we use path-wise KL for alignment and point-wise KL for composition. However, it is not obvious how to compute the point-wise KL, as evaluating the marginal densities is intractable. We next establish a similar formula as (3) by restricting the score function class.

**Lemma 2** (Point-wise KL divergence). *Assume two score functions  $s_p(x, t) = \nabla \log \bar{p}_t(x)$ ,  $s_q(x, t) = \nabla \log \bar{q}_t(x)$ , where  $\bar{p}_t$ ,  $\bar{q}_t$  are two marginal densities induced by two forward diffusion processes, with the same noise schedule, starting from initial distributions  $\bar{p}_0$  and  $\bar{q}_0$ , respectively. Then, the point-wise KL divergence between distributions of the samples generated by running DDIM with  $s_p$  and  $s_q$  is given by*

$$D_{\text{KL}}(p_0(\cdot; s_p) \parallel p_0(\cdot; s_q)) = \sum_{t=0}^T \tilde{\omega}_t \mathbb{E}_{x \sim p_t(\cdot; s_p)} \left[ \|s_p(x, t) - s_q(x, t)\|_2^2 \right] + \epsilon_T \quad (4)$$

where  $\tilde{\omega}_t$  is a time-dependent constant and  $\epsilon_T$  is a discretization error depending on the number of diffusion time steps  $T$ .

See Appendix C.2 for proof. The key intuition behind Lemma 2 is that if two diffusion processes are close, and their starting distributions are the same (e.g.,  $\mathcal{N}(0, I)$  at time  $t = T$ ), then the end points (i.e., the distributions at  $t = 0$ ) must also be close. The sum on the right hand side of (4) can be viewed as the difference of the processes over time steps.

### 3 Aligning Pretrained Model with Multiple Reward Constraints

To apply Problem (UR-A) to diffusion models, we first employ Lagrangian duality to derive its solution in the distribution space. Alignment with constraints is related but fundamentally different from the standard approach of minimizing a weighted average of the KL divergence and rewards [16]. They are related because the Lagrangian for (UR-A) is precisely a weighted average,

$$L_{\text{ALI}}(p, \lambda) := D_{\text{KL}}(p \| q) - \lambda^\top (\mathbb{E}_{x \sim p}[r(x)] - b). \quad (5)$$

where we use shorthand  $b := [b_1, \dots, b_m]^\top$ ,  $r := [r_1, \dots, r_m]^\top$ , and  $\lambda := [\lambda_1, \dots, \lambda_m]^\top$  is the Lagrangian multiplier or dual variable. Let the dual function be  $D_{\text{ALI}}(\lambda) := \underset{p \in \mathcal{P}}{\text{minimize}} L_{\text{ALI}}(p, \lambda)$  and an optimal dual variable be  $\lambda^* \in \underset{\lambda \geq 0}{\text{argmax}} D_{\text{ALI}}(\lambda)$ . Denote  $D_{\text{ALI}}^* := D_{\text{ALI}}(\lambda^*)$ . For  $\lambda > 0$ , we define a reward weighted distribution  $q_{\text{rw}}^{(\lambda)}$  as

$$q_{\text{rw}}^{(\lambda)}(\cdot) := \frac{1}{Z_{\text{rw}}(\lambda)} q(\cdot) e^{\lambda^\top r(\cdot)} \quad (6)$$

where  $Z_{\text{rw}}(\lambda) := \int q(x) e^{\lambda^\top r(x)} dx$  is a normalizing constant.

In the distribution space, Problem (UR-A) is a convex optimization problem since the KL divergence is strongly convex and the reward constraints are linear in  $p \in \mathcal{P}$ . Thus, we apply strong duality in convex optimization [4] to characterize the solution to Problem (UR-A) in Theorem 1. Moreover, it is ready to formulate the constrained alignment problem (UR-A) as an unconstrained problem by specializing the dual variable to a solution to the dual problem.

**Assumption 1** (Feasibility). *There exists a model  $p$  such that  $\mathbb{E}_{x \sim p}[r_i(x)] > b_i$  for all  $i = 1, \dots, n$ .*

**Theorem 1** (Reward alignment). *Let Assumption 1 hold. Then, Problem (UR-A) is strongly dual, i.e.,  $P_{\text{ALI}}^* = D_{\text{ALI}}^*$ . Moreover, Problem (UR-A) is equivalent to*

$$\underset{p \in \mathcal{P}}{\text{minimize}} D_{\text{KL}}(p \| q_{\text{rw}}^{(\lambda^*)}) \quad (7)$$

where  $\lambda^*$  is the optimal dual variable, and the dual function has the explicit form,  $D_{\text{ALI}}(\lambda) = -\log Z_{\text{rw}}(\lambda)$ . Furthermore, the optimal solution of (UR-A) is given by

$$p^* = q_{\text{rw}}^{(\lambda^*)}. \quad (8)$$

See Appendix C.3 for proof. Theorem 1 characterizes the solution to the constrained alignment problem (UR-A), i.e.,  $q_{\text{rw}}^{(\lambda^*)}$ . This solution generalizes the reward-tilted distribution [13], which is the solution of finetuning a model with an expected reward regularizer. In Problem (UR-A), an optimal dual variable  $\lambda^*$  weights each reward so that all the constraints are satisfied optimally, while staying as close as possible to the pretrained model.

### 3.1 Reward alignment of diffusion models

We now introduce diffusion models to Problem (UR-A) by representing  $p$  and  $q$  as two diffusion models  $p_{0:T}(\cdot; s_p)$  and  $q_{0:T}(\cdot; s_q)$ , respectively. The path-wise KL divergence has been widely used in diffusion model alignment to capture the difference between two diffusion models [16]. Hence, we can instantiate Problem (UR-A) in the function space below,

$$\begin{aligned} & \underset{s_p \in \mathcal{S}}{\text{minimize}} \quad D_{\text{KL}}(p_{0:T}(\cdot; s_p) \| q_{0:T}(\cdot; s_q)) \\ & \text{subject to} \quad \mathbb{E}_{x_0 \sim p_0(\cdot; s_p)} [r_i(x_0)] \geq b_i \quad \text{for } i = 1, \dots, m. \end{aligned} \quad (\text{SR-A})$$

We define the Lagrangian for Problem (SR-A) as  $\bar{L}_{\text{ALI}}(s_p, \lambda) := L_{\text{ALI}}(p_{0:T}(\cdot; s_p), \lambda)$ . Similarly, we denote the primal and dual values by  $\bar{P}_{\text{ALI}}^*$  and  $\bar{D}_{\text{ALI}}^*$ . Although Problem (SR-A) is a non-convex optimization problem, strong duality still holds.

**Theorem 2** (Strong duality). *Let Assumption 1 hold for some  $s \in \mathcal{S}$ . Then, Problem (SR-A) is strongly dual, i.e.,  $\bar{P}_{\text{ALI}}^* = \bar{D}_{\text{ALI}}^*$ .*

See the proof of Theorem 2 in Appendix C.4. Motivated by strong duality, we present a dual-based method for solving Problem (SR-A) in which we alternate between minimizing the Lagrangian via gradient descent steps and maximizing the dual function via dual sub-gradient ascent steps below.

**Primal minimization:** At iteration  $n$ , we obtain a new model  $s^{(n+1)}$  via a Lagrangian maximization,

$$s^{(n+1)} \in \underset{s_p \in \mathcal{S}}{\text{argmin}} \bar{L}_{\text{ALI}}(s_p, \lambda^{(n)}). \quad (9)$$

**Dual maximization:** Then, we use the model  $s^{(n+1)}$  to estimate the constraint violation  $\mathbb{E}_{x_0}[r(x_0)] - b$ , denoted as  $r(s^{(n+1)}) - b$ , and perform a dual sub-gradient ascent step,

$$\lambda^{(n+1)} = \left[ \lambda^{(n)} + \eta (r(s^{(n+1)}) - b) \right]_+. \quad (10)$$

## 4 Constrained Composition of Multiple Pretrained Models

To apply Problem (UR-C) to diffusion models, we first employ Lagrangian duality to derive its solution in the distribution space  $\mathcal{P}$ . Let the Lagrangian for Problem (UR-C) be

$$L_{\text{AND}}(p, u, \lambda) := u + \sum_{i=1}^m \lambda_i (D_{\text{KL}}(p \| q^i) - u), \quad (11)$$

and the associated dual function  $D_{\text{AND}}(\lambda)$ , which is always concave, is defined as

$$D_{\text{AND}}(\lambda) := \max_{u \in \mathbb{R}, p \in \mathcal{P}} L_{\text{AND}}(p, u, \lambda). \quad (12)$$

Let a solution to Problem (UR-A) be  $(p^*, u^*)$ , and let the optimal value of the objective function be  $P_{\text{AND}}^* = u^*$ . Let an optimal dual variable pair be  $\lambda^* \in \text{argmax}_{\lambda \geq 0} D_{\text{AND}}(\lambda)$ , and the optimal value of the dual function be  $D_{\text{AND}}^* := D_{\text{AND}}(\lambda^*)$ .

For  $\lambda > 0$ , we define a product distribution  $q_{\text{AND}}^{(\lambda)}$  as a product of  $m$  tilted distributions  $q^i$ ,

$$q_{\text{AND}}^{(\lambda)}(\cdot) := \frac{1}{Z_{\text{AND}}(\lambda)} \prod_{i=1}^m (q^i(\cdot))^{\frac{\lambda_i}{1^\top \lambda}} \quad (13)$$

where  $Z_{\text{AND}}(\lambda) := \int \prod_{i=1}^m (q^i(x))^{\frac{\lambda_i}{1^\top \lambda}} dx$  is a normalizing constant.

**Assumption 2** (Feasibility). *There exist a model  $p$  such that  $D_{\text{KL}}(p \parallel q_i) < u$  for all  $i = 1, \dots, n$ .*

Assumption 2 requires that the supports of the distributions  $q^i$  have non-empty intersection.

**Theorem 3** (Product composition). *Let Assumption 2 hold. Then, Problem (UR-C) is strongly dual, i.e.,  $P_{\text{AND}}^* = D_{\text{AND}}^*$ . Moreover, Problem (UR-C) is equivalent to*

$$\underset{p \in \mathcal{P}}{\text{minimize}} \ D_{\text{KL}}(p \parallel q_{\text{AND}}^{(\lambda^*)}) \quad (14)$$

where  $\lambda^*$  is an optimal dual variable, and the dual function has the explicit form,  $D(\lambda) = -\log Z_{\text{AND}}(\lambda)$ . Furthermore, the optimal solution of (14) is given by

$$p^* = q_{\text{AND}}^{(\lambda^*)}. \quad (15)$$

We defer the proof of Theorem 3 to Appendix C.5. The distribution  $q_{\text{AND}}^{(\lambda)} \propto \prod_{i=1}^m (q^i(\cdot))^{\frac{\lambda_i}{1^\top \lambda}}$  allows sampling from a weighted product of  $m$  distributions, where the parameters  $\{\lambda_i/1^\top \lambda\}_{i=1}^m$  weight the importance of each distribution. The geometric mean is a special case when all  $\lambda_i$  are equal [1].

**Remark 1.** Theorem 3 connects our proposed constrained optimization problem (UR-C) to the well-known problem of sampling from a product of multiple distributions [1, 14]. Furthermore, our constraints enforce that the resulting product is properly weighted to ensure the solution diverges as little as possible from each of the individual distributions (see Figure 1).

## 4.1 Product composition of diffusion models

We introduce diffusion models to Problem (UR-A) via an optimization problem in the function space,

$$\begin{aligned} & \underset{u \geq 0, s \in \mathcal{S}}{\text{minimize}} \quad u \\ & \text{subject to} \quad D_{\text{KL}}(p(x_0; s) \parallel p(x_0; s^i)) \leq u \quad \text{for } i = 1, \dots, m. \end{aligned} \quad (\text{SR-C})$$

We define a Lagrangian for Problem (SR-C) as  $\bar{L}_{\text{AND}}(s_p, u, \lambda) := L_{\text{AND}}(p(x_0; s_p), u, \lambda)$ . Similarly, we introduce the primal and dual values  $\bar{P}_{\text{AND}}^*$  and  $\bar{D}_{\text{AND}}^*$ . Although Problem (SR-C) is a non-convex optimization problem, strong duality still holds.

**Theorem 4** (Strong duality). *Let Assumption 2 hold for some  $p(\cdot; s)$  with  $s \in \mathcal{S}$ . Then, Problem (SR-C) is strongly dual, i.e.,  $\bar{P}_{\text{AND}}^* = \bar{D}_{\text{AND}}^*$ .*

See the proof of Theorem 4 in Appendix C.6. For solving the constrained optimization problem (SR-C) we can use a primal-dual approach similar to the one discussed in Section 3.1.

**Primal minimization:** At iteration  $n$ , we obtain a new model  $s^{(n+1)}$  via a Lagrangian maximization,

$$s^{(n+1)} \in \operatorname{argmin}_{s_p \in \mathcal{S}} \bar{L}_{\text{AND}}(s_p, \lambda^{(n)}). \quad (16)$$

**Dual maximization:** Then, we use the model  $s^{(n+1)}$  to estimate the constraint violation and perform a dual sub-gradient ascent step,

$$\lambda^{(n+1)} = \left[ \lambda^{(n)} + \eta \left( D_{\text{KL}}(p(x_0; s^{(n+1)}) \| p(x_0; s^i)) - u \right) \right]_+. \quad (17)$$

We note that computing the point-wise KL divergence that shows up in both the Lagrangian and the constraint violations is not trivial. Recall that Lemma 2 gives us a way to compute the point-wise KL divergence  $D_{\text{KL}}(p(x_0; s) \| p(x_0; s^i))$ . However, it requires that the functions  $s$  and  $s^i$  each be a valid score function for some process. It is reasonable to assume this is the case for  $s^i$  since it represents a pretrained model where it would have been trained to approximate the true score of a forward diffusion process. Yet regarding the function  $s$  that we are optimizing over, there is no guarantee that any given  $s \in \mathcal{S}$  is a valid score function. In spite of this, Lemma 3 lets us minimize the Lagrangian.

**Lemma 3.** *The Lagrangian for Problem (SR-C) is equivalently written as*

$$L_{\text{AND}}(s, \lambda) = D_{\text{KL}}(p(x_0; s) \| q_{\text{AND}}^{(\lambda)}(x_0)) - \log Z_{\text{AND}}(\lambda). \quad (18)$$

Furthermore, a Lagrangian minimizer  $s^{(\lambda)} := \operatorname{argmin} L_{\text{AND}}(s, \lambda)$  is given by

$$s^{(\lambda)} = \operatorname{argmin}_{s \in \mathcal{S}} \sum_{t=0}^T \omega_t \mathbb{E}_{x_0 \sim q_{\text{AND}}^{(\lambda)}(\cdot)} \mathbb{E}_{x_t \sim q(x_t | x_0)} \left[ \|s(x, t) - \nabla \log q(x_t | x_0)\|^2 \right] \quad (19)$$

where  $q(x_t | x_0) \sim \mathcal{N}(\sqrt{\bar{\alpha}_t} x_0, (1 - \bar{\alpha}_t) I)$ , and  $s^{(\lambda)} = \nabla \log q_{\text{AND}, t}^{(\lambda)}$ .

See Appendix C for proof. With Lemma 3, as long as we have access to samples from the distribution  $q_{\text{AND}}^{(\lambda)}$ , we can approximate the expectation in (19) and use gradient-based optimization methods to find the minimizer  $s^{(\lambda)}$ . To obtain these samples, we use annealed Markov Chain Monte Carlo (MCMC) sampling as proposed by [14]; see Appendix B for sampling details. For the dual update, we can evaluate the KL divergence  $D_{\text{KL}}(p_0(\cdot; s^{(\lambda)}) \| p_0(\cdot; s^i))$  between the marginal densities induced by the Lagrangian minimizer  $s^{(\lambda)}$  and the individual score functions  $s^i$  using Lemma 2 since both are valid score functions.

**Remark 2.** *In practice the primal steps will yield an approximate Lagrangian minimizer  $s^{(\tilde{\lambda})}(x, t) \approx \nabla \log q_{\text{AND}, t}^{(\lambda)}(x)$ . This results in two sources of error in evaluating the point-wise KL:*

$$D_{\text{KL}}(p_0(\cdot; s^{(\lambda)}) \| p_0(\cdot; s^i)) = \sum_{t=0}^T \tilde{\omega}_t \mathbb{E}_{x \sim p_t(\cdot; s^{(\lambda)})} \left[ \|s^{(\lambda)}(x, t) - s^i(x, t)\|_2^2 \right] + \epsilon_T \quad (20)$$

*First, the error induced by not using the exact  $s^{(\lambda)}$  in  $\|s^{(\lambda)}(x, t) - s^i(x, t)\|_2^2$ . Second, the error induced by not evaluating the expectation on correct trajectories given by  $x \sim p_t(\cdot; s^{(\lambda)})$ . However the second error can be reduced since if we have a way of sampling from the true product  $x_0 \sim q_{\text{AND}, 0}^{(\lambda)}$ , we can get samples from  $p_t(\cdot; s^{(\lambda)})$  just by adding Gaussian noise to  $x_0$ .*

See Appendix E for the detailed algorithm for product composition.

## 5 Computational Experiments

### 5.1 Finetuning to align with multiple rewards

We extend the AlignProp framework [33] to accommodate multiple reward constraints and dual updates. We finetune Stable Diffusion v1.5 <sup>2</sup> on widely used differentiable image quality and aesthetic rewards, namely aesthetic [37], hps [50], pickscore [22], imagereward [52] and mps [58]. Since these rewards have widely varying scales, which can make setting the constraint levels challenging, we normalize them by computing the average and standard deviation over a number of batches. In all experiments, models are finetuned using LoRA [20]. Experimental settings and hyperparameters are detailed in Appendix F.

**I. MPS + contrast, saturation, sharpness constraints.** A common shortcoming of several off-the-shelf aesthetics, image preference and quality reward models is their tendency to overfit to certain image characteristics such as saturation, and sharp high-contrast textures. See, for example, images in the first column in Figure 3 (right). In order to mitigate this issue, we add regularizers to the reward to explicitly penalize these characteristics. However, if the regularization weight is not carefully set, models fit these regularizers rather than the reward. As shown in Figure 3, when using equal weights the MPS reward *decreases* (left plot). In contrast, our constrained approach can effectively control multiple undesired artifacts while ensuring none of the rewards are neglected by obtaining a near feasible solution for the specified constraint level, which represents a 50% improvement.



Figure 3: We finetune stable diffusion with one reward emphasizing aesthetic quality (MPS), and Saturation and Local Contrast regularizers. Left: Value of the rewards after finetuning. Right: Images sampled from the aligned models, and the model trained solely with MPS [58] reward for comparison.

**II. Multiple aesthetic constraints.** When finetuning with multiple rewards, arbitrarily setting fixed weights can lead to disparate performance among them. This can be observed in Figure 4 (left plot), where the model overfits to one reward while neglecting the more challenging reward (hps). In contrast, constraining all rewards allows the model to improve all rewards by the desired constraint level, including challenging ones (hps). As pictured in Figure 4, minimizing the KL subject to constraints also results in lower KL to the pre-trained model (middle plot). Without constraint, due to reward overfitting the finetuned model diverges too far from the pretrained model which is undesirable (right plot).

<sup>2</sup><https://huggingface.co/stable-diffusion-v1-5/stable-diffusion-v1-5>

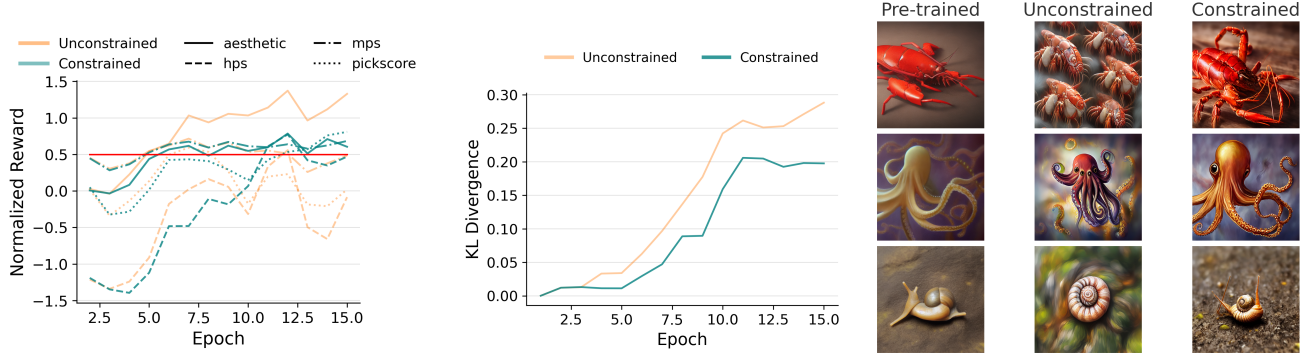


Figure 4: Finetuning with multiple image quality/aesthetic rewards. Left: Reward trajectories in training. Middle: KL to pre-trained model constrained. Right: Images sampled from the aligned models and the pre-trained model for reference.

## 5.2 Product composition of diffusion models

In high-dimensional settings like image generation, using MCMC to get samples from the true product distribution and then minimizing the Lagrangian via (19) to find the true product score function is prohibitively costly. To circumvent this, we use a surrogate for the true score both for sampling and computing the KL, as detailed in Appendix F.

**I. Composing models fine-tuned on different rewards.** We investigate the composition of multiple finetuned versions of the same base model, where each one fit LoRA adapters a different reward function. A key challenge lies in selecting appropriate weights for this combination. Arbitrary choices may lead to undesirable trade-offs and under-representation of certain models in the mixture as evidenced in Figure 5 by drops in up to 30% in some rewards. Our constrained approach gives us a way to find the weights that keep us close to each individual model, leading to higher rewards for all models.

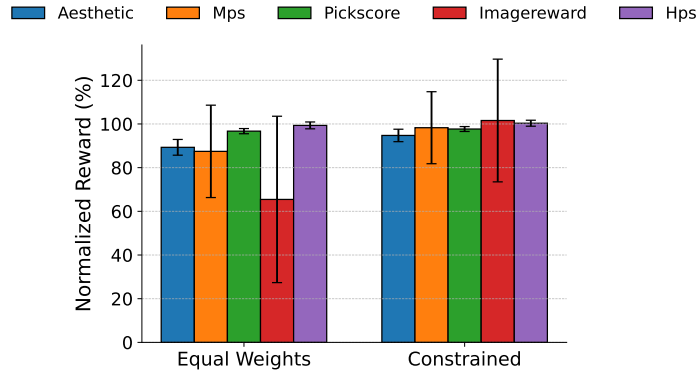


Figure 5: Composition of adapters finetuned for different rewards, for an equal weighted and product mixture. 100 represents the reward attained by the model trained with each individual reward. Higher is better.

## II. Concept composition with stable diffusion.

Following the setting in [38], we compose two text-to-image diffusion models conditioned on different

	Min. CLIP ( $\uparrow$ )	Min. BLIP ( $\uparrow$ )
Combined Prompting	22.1	0.204
Equal Weights	22.7	0.252
Constrained (Ours)	<b>22.9</b>	<b>0.268</b>

Table 1: **Comparing constrained approach to baselines on minimum CLIP and BLIP scores.** The scores are averaged over 50 different prompt pairs randomly sampled from a list of simple prompts.



Figure 6: Concept composition examples for each method. The constrained method prevents any one concept from being ignored. Prompts for each row: **1:** "a pineapple", "a volcano". **2:** "a donut", "a turtle". **3:** "a dandelion", "a spider web", "a cinnamon roll".

inputs. We use constrained learning ([SR-C](#)) to find the optimal weights to compose these two models. We compare to the baseline of using equal weights for the composition. We can see that closeness to each model also encourages the representation of the concept in the images generated by the composed model as reflected by the improved text-to-image similarity metrics CLIP [19] and BLIP [24] scores in Table 1. We compute the similarity score between the generated images and each of the two prompts and compare the minimums. We also compare to the baseline of generating images from a combined prompt that includes both prompts. See a qualitative comparison between the methods in Figure 6. Implementation details and more results can be found in Appendix F.

## 6 Concluding Remarks

We have developed a constrained optimization framework that unifies alignment and composition of diffusion models by enforcing that the aligned model satisfies reward constraints and/or remains close to each pre-trained model. We provide a theoretical characterization of the solutions to the constrained alignment and composition problems, and develop Lagrangian-based primal-dual training algorithms to approximate these solutions. Empirically, we demonstrate the effectiveness and merits of our constrained approach in image generation, applying it to alignment and composition, and show that our aligned or composed model satisfies constraints, effectively, and improves on the equally-weighted approach.

## References

- [1] B. Biggs, A. Seshadri, Y. Zou, A. Jain, A. Golatkar, Y. Xie, A. Achille, A. Swaminathan, and S. Soatto. Diffusion soup: Model merging for text-to-image diffusion models. *arXiv preprint arXiv:2406.08431*, 2024.
- [2] K. Black, M. Janner, Y. Du, I. Kostrikov, and S. Levine. Training diffusion models with reinforcement learning. In *The Twelfth International Conference on Learning Representations*, 2024.
- [3] A. Blattmann, R. Rombach, H. Ling, T. Dockhorn, S. W. Kim, S. Fidler, and K. Kreis. Align your latents: High-resolution video synthesis with latent diffusion models. In *Proceedings of the IEEE/CVF conference on computer vision and pattern recognition*, pages 22563–22575, 2023.
- [4] S. P. Boyd and L. Vandenberghe. *Convex optimization*. Cambridge university press, 2004.
- [5] A. Bradley and P. Nakkiran. Classifier-free guidance is a predictor-corrector. *arXiv preprint arXiv:2408.09000*, 2024.
- [6] L. F. Chamon, S. Paternain, M. Calvo-Fullana, and A. Ribeiro. Constrained learning with non-convex losses. *IEEE Transactions on Information Theory*, 69(3):1739–1760, 2022.
- [7] L. F. O. Chamon and A. Ribeiro. Probably approximately correct constrained learning, 2021.
- [8] J. Chen, R. Zhang, Y. Zhou, and C. Chen. Towards aligned layout generation via diffusion model with aesthetic constraints. In *The Twelfth International Conference on Learning Representations*, 2024.
- [9] C. Chi, Z. Xu, S. Feng, E. Cousineau, Y. Du, B. Burchfiel, R. Tedrake, and S. Song. Diffusion policy: Visuomotor policy learning via action diffusion. *The International Journal of Robotics Research*, page 02783649241273668, 2023.
- [10] M. Chidambaram, K. Gatmiry, S. Chen, H. Lee, and J. Lu. What does guidance do? a fine-grained analysis in a simple setting. *arXiv preprint arXiv:2409.13074*, 2024.
- [11] J. K. Christopher, S. Baek, and N. Fioretto. Constrained synthesis with projected diffusion models. *Advances in Neural Information Processing Systems*, 37:89307–89333, 2024.
- [12] K. Clark, P. Vicol, K. Swersky, and D. J. Fleet. Directly fine-tuning diffusion models on differentiable rewards. In *The Twelfth International Conference on Learning Representations*, 2024.
- [13] C. Domingo-Enrich, M. Drozdzal, B. Karrer, and R. T. Q. Chen. Adjoint matching: Fine-tuning flow and diffusion generative models with memoryless stochastic optimal control, 2025.
- [14] Y. Du, C. Durkan, R. Strudel, J. B. Tenenbaum, S. Dieleman, R. Fergus, J. Sohl-Dickstein, A. Doucet, and W. Grathwohl. Reduce, reuse, recycle: Compositional generation with energy-based diffusion models and mcmc, 2024.
- [15] Y. Fan and K. Lee. Optimizing DDPM sampling with shortcut fine-tuning. In *International Conference on Machine Learning*, pages 9623–9639. PMLR, 2023.

- [16] Y. Fan, O. Watkins, Y. Du, H. Liu, M. Ryu, C. Boutilier, P. Abbeel, M. Ghavamzadeh, K. Lee, and K. Lee. DPOK: Reinforcement learning for fine-tuning text-to-image diffusion models, 2023.
- [17] G. Giannone, A. Srivastava, O. Winther, and F. Ahmed. Aligning optimization trajectories with diffusion models for constrained design generation. *Advances in Neural Information Processing Systems*, 36:51830–51861, 2023.
- [18] Y. Han, M. Razaviyayn, and R. Xu. Stochastic control for fine-tuning diffusion models: Optimality, regularity, and convergence. *arXiv preprint arXiv:2412.18164*, 2024.
- [19] J. Hessel, A. Holtzman, M. Forbes, R. L. Bras, and Y. Choi. Clipscore: A reference-free evaluation metric for image captioning, 2022.
- [20] E. J. Hu, Y. Shen, P. Wallis, Z. Allen-Zhu, Y. Li, S. Wang, L. Wang, W. Chen, et al. Lora: Low-rank adaptation of large language models. *ICLR*, 1(2):3, 2022.
- [21] S. Khalafi, D. Ding, and A. Ribeiro. Constrained diffusion models via dual training. In *The Thirty-eighth Annual Conference on Neural Information Processing Systems*, 2024.
- [22] Y. Kirstain, A. Polyak, U. Singer, S. Matiana, J. Penna, and O. Levy. Pick-a-pic: An open dataset of user preferences for text-to-image generation. *Advances in Neural Information Processing Systems*, 36:36652–36663, 2023.
- [23] K. Lee, H. Liu, M. Ryu, O. Watkins, Y. Du, C. Boutilier, P. Abbeel, M. Ghavamzadeh, and S. S. Gu. Aligning text-to-image models using human feedback. *arXiv preprint arXiv:2302.12192*, 2023.
- [24] J. Li, D. Li, C. Xiong, and S. Hoi. Blip: Bootstrapping language-image pre-training for unified vision-language understanding and generation, 2022.
- [25] S. Li, K. Kallidromitis, A. Gokul, Y. Kato, and K. Kozuka. Aligning diffusion models by optimizing human utility. In *The Thirty-eighth Annual Conference on Neural Information Processing Systems*, 2024.
- [26] J. Liang, J. K. Christopher, S. Koenig, and F. Fioretto. Multi-agent path finding in continuous spaces with projected diffusion models. *arXiv preprint arXiv:2412.17993*, 2024.
- [27] J. Liang, J. K. Christopher, S. Koenig, and F. Fioretto. Simultaneous multi-robot motion planning with projected diffusion models. *arXiv preprint arXiv:2502.03607*, 2025.
- [28] B. Liu, S. Shao, B. Li, L. Bai, Z. Xu, H. Xiong, J. Kwok, S. Helal, and Z. Xie. Alignment of diffusion models: Fundamentals, challenges, and future. *arXiv preprint arXiv:2409.07253*, 2024.
- [29] N. Liu, S. Li, Y. Du, A. Torralba, and J. B. Tenenbaum. Compositional visual generation with composable diffusion models. In *European Conference on Computer Vision*, pages 423–439. Springer, 2022.
- [30] S. Lyu. Interpretation and generalization of score matching, 2012.
- [31] W. Mou, N. Flammarion, M. J. Wainwright, and P. L. Bartlett. Improved bounds for discretization of langevin diffusions: Near-optimal rates without convexity, 2019.

- [32] S. S. Narasimhan, S. Agarwal, L. Rout, S. Shakkottai, and S. P. Chinchali. Constrained posterior sampling: Time series generation with hard constraints. *arXiv preprint arXiv:2410.12652*, 2024.
- [33] M. Prabhudesai, A. Goyal, D. Pathak, and K. Fragkiadaki. Aligning text-to-image diffusion models with reward backpropagation, 2024.
- [34] M. Prabhudesai, R. Mendonca, Z. Qin, K. Fragkiadaki, and D. Pathak. Video diffusion alignment via reward gradients. *arXiv preprint arXiv:2407.08737*, 2024.
- [35] R. Rombach, A. Blattmann, D. Lorenz, P. Esser, and B. Ommer. High-resolution image synthesis with latent diffusion models, 2022.
- [36] C. Saharia, W. Chan, S. Saxena, L. Li, J. Whang, E. L. Denton, K. Ghasemipour, R. Gontijo Lopes, B. Karagol Ayan, T. Salimans, et al. Photorealistic text-to-image diffusion models with deep language understanding. *Advances in neural information processing systems*, 35:36479–36494, 2022.
- [37] C. Schuhmann, R. Beaumont, R. Vencu, C. Gordon, R. Wightman, M. Cherti, T. Coombes, A. Katta, C. Mullis, M. Wortsman, et al. Laion-5b: An open large-scale dataset for training next generation image-text models. *Advances in neural information processing systems*, 35:25278–25294, 2022.
- [38] M. Skreta, L. Atanackovic, J. Bose, A. Tong, and K. Neklyudov. The superposition of diffusion models using the itô density estimator. In *The Thirteenth International Conference on Learning Representations*, 2025.
- [39] M. Sohrabi, J. Ramirez, T. H. Zhang, S. Lacoste-Julien, and J. Gallego-Posada. On pi controllers for updating lagrange multipliers in constrained optimization. In *International Conference on Machine Learning*, pages 45922–45954. PMLR, 2024.
- [40] J. Song, C. Meng, and S. Ermon. Denoising diffusion implicit models, 2022.
- [41] Y. Song, J. Sohl-Dickstein, D. P. Kingma, A. Kumar, S. Ermon, and B. Poole. Score-based generative modeling through stochastic differential equations, 2021.
- [42] M. Uehara, Y. Zhao, T. Biancalani, and S. Levine. Understanding reinforcement learning-based fine-tuning of diffusion models: A tutorial and review. *arXiv preprint arXiv:2407.13734*, 2024.
- [43] M. Uehara, Y. Zhao, K. Black, E. Hajiramezanali, G. Scalia, N. L. Diamant, A. M. Tseng, T. Biancalani, and S. Levine. Fine-tuning of continuous-time diffusion models as entropy-regularized control. *arXiv preprint arXiv:2402.15194*, 2024.
- [44] M. Uehara, Y. Zhao, K. Black, E. Hajiramezanali, G. Scalia, N. L. Diamant, A. M. Tseng, S. Levine, and T. Biancalani. Feedback efficient online fine-tuning of diffusion models. In *Forty-first International Conference on Machine Learning*, 2024.
- [45] M. Uehara, Y. Zhao, E. Hajiramezanali, G. Scalia, G. Eraslan, A. Lal, S. Levine, and T. Biancalani. Bridging model-based optimization and generative modeling via conservative fine-tuning of diffusion models. *Advances in Neural Information Processing Systems*, 37:127511–127535, 2024.
- [46] A. Ulhaq and N. Akhtar. Efficient diffusion models for vision: A survey. *arXiv preprint arXiv:2210.09292*, 2022.

- [47] B. Wallace, M. Dang, R. Rafailov, L. Zhou, A. Lou, S. Purushwalkam, S. Ermon, C. Xiong, S. Joty, and N. Naik. Diffusion model alignment using direct preference optimization. In *Proceedings of the IEEE/CVF Conference on Computer Vision and Pattern Recognition*, pages 8228–8238, 2024.
- [48] L. Wang, C. Song, Z. Liu, Y. Rong, Q. Liu, and S. Wu. Diffusion models for molecules: A survey of methods and tasks. *arXiv preprint arXiv:2502.09511*, 2025.
- [49] X. Wu, Y. Hao, M. Zhang, K. Sun, Z. Huang, G. Song, Y. Liu, and H. Li. Deep reward supervisions for tuning text-to-image diffusion models. In *European Conference on Computer Vision*, pages 108–124, 2024.
- [50] X. Wu, K. Sun, F. Zhu, R. Zhao, and H. Li. Better aligning text-to-image models with human preference. *arXiv preprint arXiv:2303.14420*, 1(3), 2023.
- [51] X. Wu, K. Sun, F. Zhu, R. Zhao, and H. Li. Human preference score: Better aligning text-to-image models with human preference. In *Proceedings of the IEEE/CVF International Conference on Computer Vision*, pages 2096–2105, 2023.
- [52] J. Xu, X. Liu, Y. Wu, Y. Tong, Q. Li, M. Ding, J. Tang, and Y. Dong. Imagereward: Learning and evaluating human preferences for text-to-image generation. *Advances in Neural Information Processing Systems*, 36:15903–15935, 2023.
- [53] J. Xu, X. Liu, Y. Wu, Y. Tong, Q. Li, M. Ding, J. Tang, and Y. Dong. Imagereward: Learning and evaluating human preferences for text-to-image generation. *Advances in Neural Information Processing Systems*, 36, 2023.
- [54] J. N. Yan, J. Gu, and A. M. Rush. Diffusion models without attention. In *Proceedings of the IEEE/CVF Conference on Computer Vision and Pattern Recognition*, pages 8239–8249, 2024.
- [55] K. Yang, J. Tao, J. Lyu, C. Ge, J. Chen, W. Shen, X. Zhu, and X. Li. Using human feedback to fine-tune diffusion models without any reward model. In *Proceedings of the IEEE/CVF Conference on Computer Vision and Pattern Recognition*, pages 8941–8951, 2024.
- [56] S. Zampini, J. Christopher, L. Oneto, D. Anguita, and F. Fioretto. Training-free constrained generation with stable diffusion models. *arXiv preprint arXiv:2502.05625*, 2025.
- [57] H. Zhang and T. Xu. Towards controllable diffusion models via reward-guided exploration, 2023.
- [58] S. Zhang, B. Wang, J. Wu, Y. Li, T. Gao, D. Zhang, and Z. Wang. Learning multi-dimensional human preference for text-to-image generation. In *Proceedings of the IEEE/CVF Conference on Computer Vision and Pattern Recognition*, pages 8018–8027, 2024.
- [59] Z. Zhang, L. Shen, S. Zhang, D. Ye, Y. Luo, M. Shi, B. Du, and D. Tao. Aligning few-step diffusion models with dense reward difference learning. *arXiv preprint arXiv:2411.11727*, 2024.
- [60] H. Zhao, H. Chen, J. Zhang, D. D. Yao, and W. Tang. Scores as actions: a framework of fine-tuning diffusion models by continuous-time reinforcement learning. *arXiv preprint arXiv:2409.08400*, 2024.

## A Limitations and Broader Impact

**Limitations:** Despite offering a unified constrained learning framework and demonstrating strong empirical results, further experiments are needed to assess our method’s effectiveness on alignment and composition tasks beyond image generation, under mixed alignment and composition constraints, and in combination with inference-time techniques. Additionally, further theoretical work is needed to understand optimality of non-convex constrained optimization, convergence and sample complexity of primal-dual training algorithms.

**Broader impact:** Our method can enhance diffusion models’ compliance with diverse requirements, such as realism, safety, fairness, and transparency. By introducing a unified constrained learning framework, our work offers practical guidance for developing more reliable and responsible diffusion model training algorithms, with potential impact across applications such as content generation, robotic control, and scientific discovery.

## B Related Work

**Alignment of diffusion models.** Our constrained alignment is related to a line of work on fine-tuning diffusion models. Standard fine-tuning typically involves optimizing either a task-specific reward that encodes desired properties, or a weighted sum of this reward and a regularization term that encourages closeness to the pre-trained model; see [15, 53, 23, 51, 57, 49, 2, 12, 59] for studies using the single reward objective and [43, 60, 45, 44, 34, 16, 18] for those using the weighted sum objective. The former class of single reward-based studies focus exclusively on generating samples with higher rewards, often at the cost of generalization beyond the training data. The latter class introduces a regularization term that regulates the model to be close to the pre-trained one, while leaving the trade-off between reward and closeness unspecified; see [42] for their typical pros and cons in practice. There are three key drawbacks to using either the single reward or weighted sum objective: (i) the trade-off between reward maximization and leveraging the utility of the pre-trained model is often chosen heuristically; (ii) it is unclear whether the reward satisfies the intended constraints; and (iii) multiple constraints are not naturally encoded within a single reward function. In contrast, we formulate alignment as a constrained learning problem: minimizing deviation from the pre-trained model subject to reward constraints. This offers a more principled alternative to existing ad hoc approaches [8, 17]. Our new alignment formulation (i) offers a theoretical guarantee of an optimal trade-off between reward satisfaction and proximity to the pre-trained model, and (ii) allows for the direct imposition of multiple reward constraints. We also remark that our constrained learning approach generalizes to fine-tuning of diffusion models with preference [47, 55, 25].

**Composition of diffusion models.** Our constrained composition approach is related to prior work on compositional generation with diffusion models. When composing pre-trained diffusion models, two widely used approaches are (i) product composition (or conjunction) and (ii) mixture composition (or disjunction). In product composition, it has been observed that the diffusion process is not compositional, e.g., a weighted sum of diffusion models does not generate samples from the product of the individual target distributions [14, 5, 10]. To address this issue, the weighted sum approach has been shown to be effective when combined with additional assumptions or techniques, such as energy-based models [29, 14], MCMC sampling [14], diffusion soup [1], and superposition [38]. However, how to determine optimal weights for

the individual models is not yet fully understood. In contrast, we propose a constrained optimization framework for composing diffusion models that explicitly determines the optimal composition weights. Hence, this formulation enables an optimal trade-off among the pre-trained diffusion models. Moreover, our constrained composition approach also generalizes to mixture composition, offering advantages over prior work [29, 14, 1, 38].

**Diffusion models under constraints.** Our work is pertinent to a line of research that incorporates constraints into diffusion models. To ensure that generated samples satisfy given constraints, several ad hoc approaches have proposed that train diffusion models under hard constraints, e.g., projected diffusion models [26, 11, 27], constrained posterior sampling [32], and proximal Langevin dynamics [56]. In contrast, our constrained alignment approach focuses on expected constraints defined via reward functions and provides optimality guarantees through duality theory. A more closely related work considers constrained diffusion models with expected constraints, focusing on mixture composition [21]. In comparison, we develop new constrained diffusion models for reward alignment and product composition.

## C Proofs

For conciseness, wherever it is clear from the context we omit the time subscript:

$$D_{\text{KL}}(p_{0:T}(x_{0:T}; s_p)) = D_{\text{KL}}(p(x_{0:T}; s_p)) \quad (21)$$

### C.1 Proof of Lemma 1

*Proof.* From (2), a DDIM process is Markovian in reverse time with conditional likelihoods,

$$p(x_{t-1}|x_t; s) = \mathcal{N}\left(\sqrt{\frac{\alpha_{t-1}}{\alpha_t}}x_t + \gamma_t s(x_t, t), \sigma_t^2 I\right). \quad (22)$$

Hence, we expand the path-wise KL divergence into

$$\begin{aligned} & D_{\text{KL}}(p_{0:T}(\cdot; s_p) \| p_{0:T}(\cdot; s_q)) \\ &= \mathbb{E}_{x_{0:T} \sim p} [\log p(x_{0:T}; s_p) - \log p(x_{0:T}; s_q)] \\ &\stackrel{(a)}{=} \mathbb{E}_{x_T \sim p_{T+1}(\cdot), x_{T-1} \sim p_T(\cdot | x_T), \dots, x_0 \sim p_1(\cdot | x_1)} \left[ \sum_{t=T}^1 \log \frac{p(x_{t-1} | x_t; s_p)}{p(x_{t-1} | x_t; s_q)} \right] \\ &\stackrel{(b)}{=} \sum_{t=T}^1 \mathbb{E}_{x_T \sim p_{T+1}(\cdot), x_{T-1} \sim p_T(\cdot | x_T), \dots, x_0 \sim p_1(\cdot | x_1)} \left[ \log \frac{p(x_{t-1} | x_t; s_p)}{p(x_{t-1} | x_t; s_q)} \right] \\ &\stackrel{(c)}{=} \sum_{t=T}^1 \mathbb{E}_{x_{0:T} \sim p} [D_{\text{KL}}(p(x_{t-1} | x_t; s_p) \| p(x_{t-1} | x_t; s_q))] \\ &\stackrel{(d)}{=} \sum_{t=T}^1 \mathbb{E}_{x_t \sim p_{t+1}} \left[ \frac{\gamma_t^2}{2\sigma_t^2} \|s_p(x_t, t) - s_q(x_t, t)\|^2 \right] \\ &\stackrel{(e)}{=} \sum_{t=T}^1 \mathbb{E}_{\{p_t\}} \left[ \frac{\gamma_t^2}{2\sigma_t^2} \|s_p(x_t, t) - s_q(x_t, t)\|^2 \right] \end{aligned}$$

where (a) is due to the diffusion process, (b) is due to the exchangeable sum and integration, (c) is the definition of reverse KL divergence at time  $t$ , (d) is due to the reverse KL divergence between two Gaussians with the same covariance and means differing by  $\gamma_t(s_p(x_t, t) - s_q(x_t, t))$ , and in (e) we abbreviate  $\mathbb{E}_{x_t \sim p_{t+1}}$  as  $\mathbb{E}_{\{p_t\}}$  that is taken over the randomness of Markov process. This concludes the proof.

The equal variance and noise schedule assumption can be relaxed, leading to a different, but still tractable sum. The path-wise KL can be decomposed into a sum of  $T$  KL divergences:

$$D_{KL}(p_{0:T}(\cdot; s_p) \| p_{0:T}(\cdot; s_q)) = \sum_{t=1}^T \mathbb{E}_{x_{0:T} \sim p} [D_{KL}(p(x_{t-1} | x_t, s_p) \| p(x_{t-1} | x_t, s_q))]$$

Importantly,  $p(x_{t-1} | x_t; s_p)$  and  $p(x_{t-1} | x_t; s_q)$  are Gaussian distributions. If the noise and variance schedules are different, the KL between the two Gaussians:

$$p(x_{t-1} | x_t; s_p) = \mathcal{N} \left( \sqrt{\frac{\alpha_{t-1}}{\alpha_t}} x_t + \gamma_t s_p(x_t, t), \sigma_t^2 I \right),$$

$$p(x_{t-1} | x_t; s_q) = \mathcal{N} \left( \sqrt{\frac{\alpha'_{t-1}}{\alpha'_t}} x_t + \gamma'_t s_q(x_t, t), \sigma'^2 I \right),$$

is still tractable and given by the following:

$$\begin{aligned} D_{KL}(p(x_{t-1} | x_t; s_p) \| p(x_{t-1} | x_t; s_q)) &= \frac{1}{2} \left[ \frac{1}{\sigma_t^2} \left\| \left( \frac{\alpha_{t-1}}{\alpha_t} - \frac{\alpha'_{t-1}}{\alpha'_t} \right) x_t + \gamma_t s_p(x_t, t) - \gamma'_t s_q(x_t, t) \right\|^2 \right. \\ &\quad \left. + d \log \left( \frac{\sigma_t^2}{\sigma'^2} \right) + d \frac{\sigma_t^2}{\sigma'^2} - d \right]. \end{aligned}$$

If variance and noise schedules are the same, i.e.,  $\alpha_t = \alpha'_t$  and  $\sigma_t = \sigma'_t$ , the above reduces to  $\frac{\gamma_t^2}{2\sigma_t^2} \|s_p(x_t, t) - s_q(x_t, t)\|^2$ .  $\square$

## C.2 Proof of Lemma 2

**Proof roadmap:** The proof for Lemma 2 is quite involved, thus we have divided the proof into steps for readability.

- We begin by giving a few definitions for continuous-time diffusion processes.
- Then, in Lemma 4 we characterize how the KL divergence between the marginals of two processes changes over time.
- Using Lemma 4, we prove Lemma 5, which is the analogue of Lemma 2 in continuous time.

- Next, Lemmas 6, 7, and 8 allow us to bound the discretization error  $\epsilon_T$  incurred when going from continuous-time processes to corresponding discretized processes, which completes the proof.

**Notation guide:** In this section, we deal with continuous-time forward and reverse diffusion processes and their discretized counterparts.

- We denote the continuous-time variable  $\tau \in [0, 1]$  to differentiate it from the discrete-time indices  $t \in \{0, \dots, T\}$ , where  $t = 0$  corresponds to  $\tau = 1$  and  $t = T$  corresponds to  $\tau = 0$ .<sup>3</sup>
- We denote by  $\mathfrak{X}_\tau$  the continuous-time reverse DDIM process and by  $X_t$  the corresponding discrete-time process.
- Consistent with the main paper, we denote then forward processes with an additional bar, e.g.,  $\bar{\mathfrak{X}}_\tau$  and  $\bar{X}_t$  represent the continuous-time and discrete-time forward processes, respectively.
- We denote by  $\mathfrak{p}_\tau(x; s)$  the marginal density of continuous-time DDIM process with score predictor  $s(x, \tau)$  at time  $\tau$ . The discrete-time counterpart is denoted by  $p_t(x; s)$ .

**Continuous-time preliminaries.** Given a score predictor  $s(x, \tau): \mathbb{R}^d \times [0, 1] \rightarrow \mathbb{R}^d$ , and a noise schedule  $\alpha_\tau$  increasing from  $\alpha_0 = 0$  to  $\alpha_1 = 1$ , we define a continuous-time reverse DDIM process as the following SDE,

$$d\mathfrak{X}_\tau = \left( \frac{\dot{\alpha}_\tau}{2\alpha_\tau} \mathfrak{X}_\tau + \left( \frac{\dot{\alpha}_\tau}{2\alpha_\tau} + \frac{\sigma_\tau^2}{2} \right) s(\mathfrak{X}_\tau, \tau) \right) dt + \sigma_\tau d\mathfrak{B}_\tau, \quad \text{for } \mathfrak{X}_0 \sim \mathcal{N}(0, I) \text{ and } \tau \in [0, 1] \quad (23)$$

where  $\mathfrak{B}_\tau$  is standard  $d$ -dimensional Brownian motion. The variance schedule  $\sigma_\tau$  is arbitrary and determines the randomness of the trajectories (e.g., if  $\sigma_\tau = 0$  for all  $\tau$ , then the trajectories will be deterministic). The DDIM generative process (23) induces marginal densities  $\mathfrak{p}_\tau(x, s)$  for  $\tau \in [0, 1]$ . Recall the discrete-time DDIM process defined in the main paper,

$$X_{t-1} = \sqrt{\frac{\alpha_{t-1}}{\alpha_t}} X_t + \gamma_t s(X_t, t) + \sigma_t \epsilon_t \quad \text{for } t \in \{1, \dots, T\}. \quad (24)$$

Up to the first-order approximation, the discrete-time process (24) is the Euler-Maruyama discretization of the continuous-time process (23), assuming a uniform discretization of time, i.e.,  $\tau = 1 - \frac{t}{T}$  (See [13] Appendix B.1 for a full derivation).

Given random variables  $\bar{\mathfrak{X}}_0 \sim \bar{\mathfrak{p}}_0 = \mathcal{N}(0, I)$  and  $\bar{\mathfrak{X}}_1 \sim \bar{\mathfrak{p}}_1$ , where  $\bar{\mathfrak{p}}_1$  is some probability distribution (e.g., the data distribution), we define a reference flow  $\bar{\mathfrak{X}}_\tau$  as

$$\bar{\mathfrak{X}}_\tau = \bar{\beta}_\tau \bar{\mathfrak{X}}_0 + \bar{\alpha}_\tau \bar{\mathfrak{X}}_1 \quad \text{for } \tau \in [0, 1]. \quad (25)$$

Note that there is no specific process implied by the definition above, since different processes can have the same marginal densities as the reference flow at all times  $\tau$ . We denote by  $\bar{\mathfrak{p}}_\tau(\cdot)$  the density of  $\bar{\mathfrak{X}}_\tau$ . As  $\bar{\alpha}_\tau$  increases from  $\bar{\alpha}_0 = 0$  to  $\bar{\alpha}_1 = 1$ , and  $\bar{\beta}_\tau$  decreases from  $\bar{\beta}_0 = 1$  to  $\bar{\beta}_1 = 0$ , the reference flow gives an interpolation between pure Gaussian noise  $\bar{\mathfrak{p}}_0 = \mathcal{N}(0, I)$  and  $\bar{\mathfrak{p}}_1$ .

---

<sup>3</sup>For consistency with other works from whom we will utilize some results in our proofs, namely [13, 30], the direction of time we consider in continuous time is reversed compared to discrete time. This does not affect any of our derivations and results beyond a minor change in notation.

If  $s(x, \tau) = \nabla_x \log \bar{p}_\tau(x)$ , then the DDIM process (23) has the same marginals as the reference flow (25), i.e.,  $\mathfrak{p}_\tau(x, s) = \bar{p}_\tau(x)$  for  $\tau \in [0, 1]$ . This assumes proper choice of  $\bar{\alpha}_\tau$  and  $\bar{\beta}_\tau$ , i.e.,  $\bar{\alpha}_\tau = \sqrt{\alpha_\tau}$  and  $\bar{\beta}_\tau = \sqrt{1 - \alpha_\tau}$ .

Lastly, the Fisher divergence between distributions  $p$  and  $q$  is defined as

$$D_F(p \parallel q) := \int p(x) \|\nabla \log p(x) - \nabla \log q(x)\|^2 dx.$$

We next generalize [30, Theorem 1] to show how the KL divergence between the marginals of two continuous-time forward processes changes at a rate governed by the Fisher divergence.

**Lemma 4.** *Let the marginal densities of  $\bar{\mathfrak{X}}_\tau$  when  $\bar{\mathfrak{X}}_1 \sim \bar{p}_1$  and  $\bar{\mathfrak{X}}_1 \sim \bar{q}_1$  be  $\bar{p}_\tau(\cdot)$  and  $\bar{q}_\tau(\cdot)$ , respectively. Then,*

$$\frac{d}{d\tau} D_{\text{KL}}(\bar{p}_\tau(\cdot) \parallel \bar{q}_\tau(\cdot)) = -\zeta_\tau \dot{\zeta}_\tau D_F(\bar{p}_\tau(\cdot) \parallel \bar{q}_\tau(\cdot)) \quad (26)$$

where  $\zeta_\tau := \bar{\beta}_\tau / \bar{\alpha}_\tau$ .

*Proof.* We start by defining  $\bar{\mathfrak{Y}}_\tau$  as a time-dependent scaling of  $\bar{\mathfrak{X}}_\tau$ ,

$$\bar{\mathfrak{Y}}_\tau := \frac{1}{\bar{\alpha}_\tau} \bar{\mathfrak{X}}_\tau = \zeta_\tau \bar{\mathfrak{X}}_0 + \bar{\mathfrak{X}}_1$$

where  $\zeta_\tau := \bar{\beta}_\tau / \bar{\alpha}_\tau$ . Denote by  $\tilde{p}_\tau(\bar{\mathfrak{Y}}_\tau)$ , the marginal density of  $\bar{\mathfrak{Y}}_\tau$  when  $\bar{\mathfrak{X}}_1 \sim \mathfrak{p}_1$  and similarly  $\tilde{q}_\tau(\bar{\mathfrak{Y}}_\tau)$ , the marginal density of  $\bar{\mathfrak{Y}}_\tau$  when  $\bar{\mathfrak{X}}_1 \sim \mathfrak{q}_1$ . We now generalize [30, Theorem 1] to show that (26) holds for  $\tilde{p}_\tau$  and  $\tilde{q}_\tau$ . We note that this theorem is for a specific case when  $\zeta_\tau = \sqrt{1 - \tau}$ . We now present Lemmas 4.1 and 4.2 which we will need in the remainder of the proof.

**Lemma 4.1.** *For density  $\tilde{p}_\tau(\bar{\mathfrak{Y}}_\tau)$  as defined above, the following identity holds:*

$$\frac{d}{dt} \tilde{p}_\tau(\bar{\mathfrak{Y}}_\tau) = \zeta_\tau \dot{\zeta}_\tau \Delta_{\bar{\mathfrak{Y}}_\tau} \tilde{p}_\tau(\bar{\mathfrak{Y}}_\tau). \quad (27)$$

where  $\Delta_x$  represents the Laplacian operator with respect to  $x$ .

*Proof of Lemma 4.1.* We start with an explicit expression for  $\tilde{p}_\tau(\bar{\mathfrak{Y}}_\tau)$ , which is the convolution of a Gaussian distribution with  $\mathfrak{p}_1(\bar{\mathfrak{X}}_1)$ ,

$$\tilde{p}_\tau(\bar{\mathfrak{Y}}_\tau) = \int_{\bar{\mathfrak{X}}_1} \frac{1}{(2\pi\zeta_\tau^2)^{d/2}} \exp\left(-\frac{\|\bar{\mathfrak{Y}}_\tau - \bar{\mathfrak{X}}_1\|^2}{2\zeta_\tau^2}\right) \mathfrak{p}_1(\bar{\mathfrak{X}}_1) d\bar{\mathfrak{X}}_1.$$

Taking the derivative of  $\tilde{p}_\tau(\bar{\mathfrak{Y}}_\tau)$  with respect to  $\tau$  leads to

$$\begin{aligned} \frac{d}{d\tau} \tilde{p}_\tau(\bar{\mathfrak{Y}}_\tau) &= \int_{\bar{\mathfrak{X}}_1} \frac{\dot{\zeta}_\tau \|\bar{\mathfrak{Y}}_\tau - \bar{\mathfrak{X}}_1\|^2}{\zeta_\tau^3} \frac{1}{(2\pi\zeta_\tau^2)^{d/2}} \exp\left(-\frac{\|\bar{\mathfrak{Y}}_\tau - \bar{\mathfrak{X}}_1\|^2}{2\zeta_\tau^2}\right) \mathfrak{p}_1(\bar{\mathfrak{X}}_1) d\bar{\mathfrak{X}}_1 \\ &\quad - \int_{\bar{\mathfrak{X}}_1} \frac{d}{\zeta_\tau} \frac{\dot{\zeta}_\tau}{(2\pi\zeta_\tau^2)^{d/2}} \exp\left(-\frac{\|\bar{\mathfrak{Y}}_\tau - \bar{\mathfrak{X}}_1\|^2}{2\zeta_\tau^2}\right) \mathfrak{p}_1(\bar{\mathfrak{X}}_1) d\bar{\mathfrak{X}}_1. \end{aligned} \quad (28)$$

On the other hand, taking the gradient of  $\tilde{p}_\tau(\bar{\mathfrak{Y}}_\tau)$  with respect to  $\bar{\mathfrak{Y}}_\tau$  leads to

$$\nabla_{\bar{\mathfrak{Y}}_\tau} \tilde{p}_\tau(\bar{\mathfrak{Y}}_\tau) = - \int_{\bar{\mathfrak{X}}_1} \frac{\bar{\mathfrak{Y}}_\tau - \bar{\mathfrak{X}}_1}{\zeta_\tau^2} \frac{1}{(2\pi\zeta_\tau^2)^{d/2}} \exp\left(-\frac{\|\bar{\mathfrak{Y}}_\tau - \bar{\mathfrak{X}}_1\|^2}{2\zeta_\tau^2}\right) \mathfrak{p}_1(\bar{\mathfrak{X}}_1) d\bar{\mathfrak{X}}_1.$$

Taking the divergence of the gradient, we get:

$$\begin{aligned}\Delta_{\bar{\mathfrak{Y}}_\tau} \tilde{\mathfrak{p}}_\tau(\bar{\mathfrak{Y}}_\tau) &= \int_{\bar{\mathfrak{X}}_1} \frac{\|\bar{\mathfrak{Y}}_\tau - \bar{\mathfrak{X}}_1\|^2}{\zeta_\tau^4} \frac{1}{(2\pi\zeta_\tau^2)^{d/2}} \exp\left(-\frac{\|\bar{\mathfrak{Y}}_\tau - \bar{\mathfrak{X}}_1\|^2}{2\zeta_\tau^2}\right) \mathfrak{p}_1(\bar{\mathfrak{X}}_1) d\bar{\mathfrak{X}}_1 \\ &\quad - \int_{\bar{\mathfrak{X}}_1} \frac{d}{\zeta_\tau^2} \frac{1}{(2\pi\zeta_\tau^2)^{d/2}} \exp\left(-\frac{\|\bar{\mathfrak{Y}}_\tau - \bar{\mathfrak{X}}_1\|^2}{2\zeta_\tau^2}\right) \mathfrak{p}_1(\bar{\mathfrak{X}}_1) d\bar{\mathfrak{X}}_1.\end{aligned}\tag{29}$$

Comparing the scaling coefficients of (28) and (29) proves the result.  $\square$

**Lemma 4.2.** *For any positive valued function  $f(x): \mathbb{R}^d \rightarrow \mathbb{R}$  whose gradient  $\nabla_x f$  and Laplacian  $\Delta_x f$  are well defined, we have*

$$\frac{\Delta_x f(x)}{f(x)} = \Delta_x \log f(x) + \|\nabla_x \log f(x)\|^2. \tag{30}$$

We now continue with the proof of Lemma 4. We start with the definition of Fisher divergence for generic distributions  $p, q$ ,

$$\begin{aligned}D_F(p \parallel q) &:= \int_x p(x) \|\nabla \log p(x) - \nabla \log q(x)\|^2 dx \\ &= \int_x p(x) \left\| \frac{\nabla p(x)}{p(x)} - \frac{\nabla q(x)}{q(x)} \right\|^2 dx \\ &= \int_x p(x) \left( \left\| \frac{\nabla p(x)}{p(x)} \right\|^2 + \left\| \frac{\nabla q(x)}{q(x)} \right\|^2 - 2 \frac{\nabla p(x)^\top \nabla q(x)}{p(x)q(x)} \right) dx.\end{aligned}\tag{31}$$

We apply integration by parts to the third term. For any open bounded subset  $\Omega$  of  $\mathbb{R}^d$  with a piecewise smooth boundary  $\Gamma = \partial\Omega$ ,

$$\begin{aligned}\int_{x \in \Omega} \nabla p(x)^\top \frac{\nabla q(x)}{q(x)} dx &= \int_{x \in \Omega} \nabla p(x)^\top (\nabla \log q(x)) dx \\ &= - \int_{x \in \Omega} p(x) \Delta \log q(x) dx + \int_{\Gamma} p(x) (\nabla \log q(x)^\top \hat{n}) d\Gamma.\end{aligned}\tag{32}$$

Assume that  $p(x)$  and  $q(x)$  are smooth and fast-decaying,

$$\int_{\Gamma} p(x) (\nabla \log q(x)^\top \hat{n}) d\Gamma \rightarrow 0.$$

Then, the boundary term in (32) vanishes. We now can combine (31) and (32) to obtain

$$D_F(p \parallel q) = \int_x p(x) \left( \|\nabla \log p(x)\|^2 + \|\nabla \log q(x)\|^2 + 2\Delta_x \log q(x) \right) dx. \tag{33}$$

Returning to our distributions  $\tilde{\mathfrak{p}}_\tau(\bar{\mathfrak{Y}}_\tau)$  and  $\tilde{\mathfrak{q}}_\tau(\bar{\mathfrak{Y}}_\tau)$ , we can rewrite (33) as

$$D_F(\tilde{\mathfrak{p}}_\tau(\cdot) \parallel \tilde{\mathfrak{q}}_\tau(\cdot)) = \int_{\bar{\mathfrak{Y}}_\tau} \tilde{\mathfrak{p}}_\tau(\bar{\mathfrak{Y}}_\tau) \left( \|\nabla \log \tilde{\mathfrak{p}}_\tau(\bar{\mathfrak{Y}}_\tau)\|^2 + \|\nabla \log \tilde{\mathfrak{q}}_\tau(\bar{\mathfrak{Y}}_\tau)\|^2 + 2\Delta_{\bar{\mathfrak{Y}}_\tau} \log \tilde{\mathfrak{q}}_\tau(\bar{\mathfrak{Y}}_\tau) \right) d\bar{\mathfrak{Y}}_\tau \tag{34}$$

For conciseness, we drop references to variables  $\bar{\mathfrak{Y}}_\tau$  and  $\bar{\mathfrak{X}}_1$  in the integration, the density functions, and the operators, whenever this does not lead to ambiguity. We start by applying Lemma 4.2 to (33),

$$\begin{aligned} D_F(\tilde{p} \parallel \tilde{q}) &= \int \tilde{p} (|\nabla \log \tilde{p}|^2 + |\nabla \log \tilde{q}|^2 + 2\Delta \log \tilde{q}), \\ &= \int \tilde{p} \left( |\nabla \log \tilde{p}|^2 + \frac{\Delta \tilde{q}}{\tilde{q}} + \Delta \log \tilde{q} \right). \end{aligned} \quad (35)$$

Next, we expand the derivative of the KL divergence into

$$\frac{d}{d\tau} D_{\text{KL}}(\tilde{p} \parallel \tilde{q}) = \int \frac{d}{d\tau} \tilde{p} \log \frac{\tilde{p}}{\tilde{q}} + \int \tilde{p} \frac{d}{d\tau} \log \tilde{p} - \int \tilde{p} \frac{d}{d\tau} \log \tilde{q}.$$

We can eliminate the second term by exchanging integration and differentiation of  $\tau$ ,

$$\int \tilde{p} \frac{d}{d\tau} \log \tilde{p} = \int \frac{d\tilde{p}}{d\tau} = \frac{d}{d\tau} \int \tilde{p} = 0.$$

As a result, there are three remaining terms in computing  $\frac{d}{d\tau} D_{\text{KL}}(\tilde{p} \parallel \tilde{q})$ , which we can further substitute using Lemma 4.1, as

$$\begin{aligned} \frac{d}{d\tau} D_{\text{KL}}(\tilde{p} \parallel \tilde{q}) &= \int \frac{d}{d\tau} \tilde{p} \log \tilde{p} - \int \frac{d}{d\tau} \tilde{p} \log \tilde{q} - \int \tilde{p} \frac{d}{d\tau} \log \tilde{q} \\ &= \zeta_\tau \dot{\zeta}_\tau \left( \int \Delta \tilde{p} \log \tilde{p} - \int \Delta \tilde{p} \log \tilde{q} - \int \tilde{p} \frac{\Delta \tilde{q}}{\tilde{q}} \right). \end{aligned} \quad (36)$$

Using integration by parts, the first term in (36) is changed to:

$$\int \Delta \tilde{p} \log \tilde{p} = \sum_{i=1}^d \frac{\partial \tilde{p}}{\partial y_i} \log \tilde{p}(y) \Big|_{y_i=\infty}^{y_i=-\infty} - \int \nabla \tilde{p}^T \nabla \log \tilde{p}.$$

The limits in the first term become zero given the smoothness and fast decay properties of  $\tilde{p}$ . The remaining term can be further simplified as

$$\int \nabla \tilde{p}^T \nabla \log \tilde{p} = \int \tilde{p} (\nabla \log \tilde{p})^T \nabla \log \tilde{p} = \int \tilde{p} |\nabla \log \tilde{p}|^2.$$

The second term in (36) can be manipulated similarly, by first using integration by parts to get

$$\int \Delta \tilde{p} \log \tilde{q} = \sum_{i=1}^d \frac{\partial \tilde{p}}{\partial y_i} \log \tilde{q} \Big|_{y_i=\infty}^{y_i=-\infty} - \int \nabla \tilde{p}^T \nabla \log \tilde{q}.$$

Applying integration by parts again to  $\nabla \tilde{p}^T \nabla \log \tilde{q}$ , we have:

$$\int \nabla \tilde{p}^T \nabla \log \tilde{q} = \sum_{i=1}^d \tilde{p} \frac{\partial \log \tilde{q}}{\partial y_i} \Big|_{y_i=\infty}^{y_i=-\infty} - \int \tilde{p} \Delta \log \tilde{q}.$$

The limits at the boundary values are all zero due to the smoothness and fast decay properties of  $\tilde{q}$ . Now collecting all terms, we have  $\int \tilde{p} \log \tilde{p} = - \int \tilde{p} |\nabla \log \tilde{p}|^2$  and  $\int \tilde{p} \log \tilde{q} = \int \tilde{p} \Delta \log \tilde{q}$ . Thus (36) becomes:

$$\frac{d}{d\tau} D_{\text{KL}}(\tilde{p} \parallel \tilde{q}) = -\zeta_\tau \dot{\zeta}_\tau \int \tilde{p} \left( |\nabla \log \tilde{p}|^2 + \Delta \log \tilde{q} + \frac{\Delta \tilde{q}}{\tilde{q}} \right).$$

Combining with (35) leads to

$$\frac{d}{d\tau} D_{\text{KL}}(\tilde{p}_\tau \| \tilde{q}_\tau) = -\zeta_\tau \dot{\zeta}_\tau D_{\text{F}}(\tilde{p}_\tau \| \tilde{q}_\tau). \quad (37)$$

Again, replacing  $\tilde{p}_\tau, \tilde{q}_\tau$  with the marginals of diffusion processes we get

$$\frac{d}{d\tau} D_{\text{KL}}(\tilde{\mathbf{p}}_\tau(\cdot) \| \tilde{\mathbf{q}}_\tau(\cdot)) = -\zeta_\tau \dot{\zeta}_\tau D_{\text{F}}(\tilde{\mathbf{p}}_\tau(\cdot) \| \tilde{\mathbf{q}}_\tau(\cdot)). \quad (38)$$

Recall that  $\tilde{\mathbf{p}}_\tau(\cdot)$  and  $\tilde{\mathbf{q}}_\tau(\cdot)$  are the densities of the scaled random variable  $\tilde{\mathbf{Y}}_\tau = \frac{1}{\tilde{\alpha}_\tau} \tilde{\mathbf{X}}_\tau$ . This leads to  $\mathbf{p}_\tau(\tilde{\mathbf{X}}_\tau) d\tilde{\mathbf{X}}_\tau = \tilde{\mathbf{p}}_\tau(\tilde{\mathbf{Y}}_\tau) d\tilde{\mathbf{Y}}_\tau$ . Thus, it is straightforward to show that both KL divergence and Fisher divergence are invariant to the scaling of the underlying random variables,

$$\begin{aligned} D_{\text{KL}}(\tilde{\mathbf{p}}_\tau(\cdot) \| \tilde{\mathbf{q}}_\tau(\cdot)) &= \int \tilde{\mathbf{p}}_\tau(\tilde{\mathbf{Y}}_\tau) \log \frac{\tilde{\mathbf{p}}_\tau(\tilde{\mathbf{Y}}_\tau)}{\tilde{\mathbf{q}}_\tau(\tilde{\mathbf{Y}}_\tau)} d\tilde{\mathbf{Y}}_\tau = \int \mathbf{p}_\tau(\tilde{\mathbf{X}}_\tau) \log \frac{\mathbf{p}_\tau(\tilde{\mathbf{X}}_\tau)}{\mathbf{q}_\tau(\tilde{\mathbf{X}}_\tau)} d\tilde{\mathbf{X}}_\tau = D_{\text{KL}}(\mathbf{p}_\tau(\cdot) \| \mathbf{q}_\tau(\cdot)), \\ D_{\text{F}}(\tilde{\mathbf{p}}_\tau(\cdot) \| \tilde{\mathbf{q}}_\tau(\cdot)) &= \int \tilde{\mathbf{p}}_\tau(\tilde{\mathbf{Y}}_\tau) \left\| \frac{\nabla \tilde{\mathbf{p}}_\tau(\tilde{\mathbf{Y}}_\tau)}{\tilde{\mathbf{p}}_\tau(\tilde{\mathbf{Y}}_\tau)} - \frac{\nabla \tilde{\mathbf{q}}_\tau(\tilde{\mathbf{Y}}_\tau)}{\tilde{\mathbf{q}}_\tau(\tilde{\mathbf{Y}}_\tau)} \right\|^2 d\tilde{\mathbf{Y}}_\tau \\ &= \int \mathbf{p}_\tau(\tilde{\mathbf{X}}_\tau) \left\| \frac{\nabla \mathbf{p}_\tau(\tilde{\mathbf{X}}_\tau)}{\mathbf{p}_\tau(\tilde{\mathbf{X}}_\tau)} - \frac{\nabla \mathbf{q}_\tau(\tilde{\mathbf{X}}_\tau)}{\mathbf{q}_\tau(\tilde{\mathbf{X}}_\tau)} \right\|^2 d\tilde{\mathbf{X}}_\tau = D_{\text{F}}(\mathbf{p}_\tau(\cdot) \| \mathbf{q}_\tau(\cdot)). \end{aligned}$$

Thus we can replace the divergences in (37) with those of the non-scaled distributions  $\bar{\mathbf{p}}_\tau(\cdot), \bar{\mathbf{q}}_\tau(\cdot)$ , which concludes the proof.  $\square$

We now present the continuous-time analogue of Lemma 2 which characterizes the point-wise KL divergence of two continuous time diffusion processes:

**Lemma 5.** *Let the marginal densities of  $\tilde{\mathbf{X}}_\tau$  when  $\tilde{\mathbf{X}}_1 \sim \bar{\mathbf{p}}_1$  and  $\tilde{\mathbf{X}}_1 \sim \bar{\mathbf{q}}_1$  be  $\bar{\mathbf{p}}_\tau(\cdot)$  and  $\bar{\mathbf{q}}_\tau(\cdot)$ , respectively. Denote their score predictors by  $s_{\mathbf{p}}(x, \tau) = \nabla_x \log \bar{\mathbf{p}}_\tau(x)$  and  $s_{\mathbf{q}}(x, \tau) = \nabla_x \log \bar{\mathbf{q}}_\tau(x)$ . Then, the point-wise KL divergence between two distributions of the samples generated by running continuous time DDIM (23) with  $s_{\mathbf{p}}$  and  $s_{\mathbf{q}}$  is given by*

$$D_{\text{KL}}(\mathbf{p}_1(\cdot; s_{\mathbf{p}}) \| \mathbf{p}_1(\cdot; s_{\mathbf{q}})) = \int_{\tau=0}^1 \omega_\tau \mathbb{E}_{x \sim \mathbf{p}_\tau(\cdot; s_{\mathbf{p}})} \left[ \|s_{\mathbf{p}}(x, \tau) - s_{\mathbf{q}}(x, \tau)\|_2^2 \right] \quad (39)$$

where  $\omega_\tau$  is a time-dependent constant.

*Proof.* We begin by leveraging the fact that since  $s_{\mathbf{p}}(x, \tau) = \nabla_x \log \bar{\mathbf{p}}_\tau(x)$ ,  $s_{\mathbf{q}}(x, \tau) = \nabla_x \log \bar{\mathbf{q}}_\tau(x)$ , then the DDIM processes and the reference flows have the same marginals, i.e.,  $\mathbf{p}_1(\cdot; s_{\mathbf{p}}) = \bar{\mathbf{p}}_1(\cdot)$  and

$\mathfrak{p}_1(\cdot; s_{\mathfrak{q}}) = \bar{\mathfrak{q}}_1(\cdot)$ . Using this we can write

$$D_{\text{KL}}(\mathfrak{p}_1(\cdot; s_{\mathfrak{p}}) \| \mathfrak{p}_1(\cdot; s_{\mathfrak{q}})) = D_{\text{KL}}(\bar{\mathfrak{p}}_1 \| \bar{\mathfrak{q}}_1) \quad (40)$$

$$= D_{\text{KL}}(\bar{\mathfrak{p}}_0 \| \bar{\mathfrak{q}}_0) - \int_0^1 \dot{\zeta}_\tau \zeta_\tau D_{\text{F}}(\bar{\mathfrak{p}}_\tau \| \bar{\mathfrak{q}}_\tau) d\tau \quad (41)$$

$$= - \int_0^1 \dot{\zeta}_\tau \zeta_\tau \mathbb{E}_{x \sim \bar{\mathfrak{p}}_\tau} \left[ \|\nabla \log \bar{\mathfrak{p}}_\tau(x) - \nabla \log \bar{\mathfrak{q}}_\tau(x)\|_2^2 \right] d\tau \quad (42)$$

$$= - \int_0^1 \dot{\zeta}_\tau \zeta_\tau \mathbb{E}_{x \sim \mathfrak{p}_\tau(\cdot; s_{\mathfrak{p}})} \left[ \|s_{\mathfrak{p}}(x, \tau) - s_{\mathfrak{q}}(x, \tau)\|_2^2 \right] d\tau \quad (43)$$

$$= \int_0^1 \frac{\dot{\alpha}_\tau}{2\alpha_\tau^2} \mathbb{E}_{x \sim \mathfrak{p}_\tau(\cdot; s_{\mathfrak{p}})} \left[ \|s_{\mathfrak{p}}(x, \tau) - s_{\mathfrak{q}}(x, \tau)\|_2^2 \right] d\tau \quad (44)$$

where (41) is a direct application of Lemma 4. To go from (41) to (42), we used the definition of Fisher divergence and the fact that  $\mathfrak{p}_0(\cdot) = \mathfrak{q}_0(\cdot) = \mathcal{N}(0, I)$ , therefore  $D_{\text{KL}}(\mathfrak{p}_0(\cdot) \| \mathfrak{q}_0(\cdot)) = 0$ . Then (43) follows from our definition of the score functions and the fact that  $\mathfrak{p}_\tau(\cdot; s_{\mathfrak{p}}) = \bar{\mathfrak{p}}_\tau(\cdot)$ . Finally, in (44) we used the fact that  $\dot{\zeta}_\tau \zeta_\tau = -\frac{\dot{\alpha}_\tau}{2\alpha_\tau^2}$  which follows from  $\zeta_\tau = \bar{\beta}_\tau / \bar{\alpha}_\tau$  and  $\bar{\alpha}_\tau = \sqrt{\alpha_\tau}, \bar{\beta}_\tau = \sqrt{1 - \alpha_\tau}$ . We define  $\omega_\tau := \frac{\dot{\alpha}_\tau}{2\alpha_\tau^2}$  to conclude the proof.  $\square$

We now turn to bridging the gap between continuous and discrete times. In [31], they bound this gap which arises from the discretization of the continuous time diffusion process. We will utilize the main result from this paper with a minor modification in that we consider a time-dependent drift term. This is formalized in Lemma 6 which lets us bound the KL divergence between the marginals  $p_t(\cdot)$  of the discrete time backward DDIM process and the corresponding marginal  $\mathfrak{p}_{t/T}(\cdot)$  of the continuous time backward process. We first define the time-dependent drift  $b_\tau : \mathbb{R}^d \rightarrow \mathbb{R}^d$  of the diffusion process (23) as

$$b_\tau(x) := \left( \frac{\dot{\alpha}_\tau}{2\alpha_\tau} x + \left( \frac{\dot{\alpha}_\tau}{2\alpha_\tau} + \frac{\sigma_\tau^2}{2} \right) s(x, \tau) \right).$$

**Assumption 3.** *The drift  $b_\tau(\cdot)$  satisfies the following properties for all times  $\tau \in [0, 1]$ ,*

1. **Lipschitz drift term.** *There is a finite constant  $L_1$  such that*

$$\|b_\tau(x) - b_\tau(y)\|_2 \leq L_1 \|x - y\|_2 \quad \text{for all } x, y \in \mathbb{R}^d. \quad (45)$$

2. **Smooth drift term.** *There is a finite constant  $L_2$  such that*

$$\|\nabla b_\tau(x) - \nabla b_\tau(y)\|_\infty \leq L_2 \|x - y\|_2 \quad \text{for all } x, y \in \mathbb{R}^d. \quad (46)$$

3. **Distant dissipativity.** *There exist strictly positive constants  $\mu, \beta$  such that*

$$\langle b_\tau(x), x \rangle \leq -\mu \|x\|_2^2 + \beta \quad \text{for all } x \in \mathbb{R}^d. \quad (47)$$

4. **Time-continuous drift term.** *There is a finite constant  $L_3$  such that*

$$\left\| \frac{\partial b_\tau(x)}{\partial \tau} \right\|_2 \leq L_3 \quad \text{for all } x \in \mathbb{R}^d. \quad (48)$$

There is an additional assumption in [31] on the smoothness of the initial densities of the continuous and discrete processes. In our case both are the standard Gaussian which satisfies the assumption.

**Lemma 6.** (*Modification of Theorem 1 from [31].*) *Let Assumption 3 hold. Then the KL divergence between the marginals of the discrete time backward process  $p_t(\cdot)$  and continuous time backward process  $\mathfrak{p}_{t/T}(\cdot)$  can be bounded as follows:*

$$D_{\text{KL}}(p_t(\cdot; s_p) \parallel \mathfrak{p}_{1-t/T}(\cdot; s_p)) \leq \frac{c}{T^2} \quad (49)$$

where  $c$  is a constant depending on the constants  $L_1, L_2, L_3, \mu, \beta$  from the assumption.

*Proof.* We do not provide the whole proof here as it would consist of almost the entirety of [31]. We focus on a small part of the proof, that is the only part that changes when we use a time-dependent drift  $b_\tau(x)$  as opposed to [31] where they assume a time-independent drift  $b(x)$ .

Consistent with their notation, we define a continuous time diffusion process:

$$dX_\tau = b_\tau(X_\tau)d\tau + dB_\tau, \quad (50)$$

and its Euler-Maruyama discretization parameterized by step size  $\eta > 0$  (In our case  $\eta = \frac{1}{T}$ ):

$$\hat{X}_{(k+1)\eta} = \hat{X}_{k\eta} + \eta b_{k\eta}(\hat{X}_{k\eta}) + \sqrt{\eta}\xi_k, \quad \xi_k \sim \mathcal{N}(0, I) \quad (51)$$

Furthermore they construct a continuous time stochastic process over the interval  $\tau \in [\eta, (k+1)\eta]$  that interpolates (51):

$$\hat{X}_\tau := \hat{X}_{k\eta} + \int_0^{\tau-k\eta} b_{k\eta}(\hat{X}_{k\eta})ds + \int_{k\eta}^\tau d\hat{B}_s \quad (52)$$

Then they prove that the densities of the two continuous time processes given by (50),(52) denoted as  $\pi_\tau$  and  $\hat{\pi}_\tau$  respectively satisfy the following (Lemma 2 from [31]):

$$\frac{d}{d\tau} D_{\text{KL}}(\hat{\pi}_\tau \parallel \pi_\tau) \leq \frac{1}{2} \int_{\mathbb{R}^d} \hat{\pi}_\tau(x) \left\| \hat{b}_\tau(x) - b_\tau(x) \right\|_2^2 dx. \quad (53)$$

where  $\hat{b}_\tau(x) := \mathbb{E} \left[ b_{k\eta}(\hat{X}_{k\eta}) \mid \hat{X}_\tau = x \right]$  where the expectation is over the process (52). Then they proceed to bound the norm inside the integral. The next equation based on equation (18) from [31] is where the time dependence of the drift term in our case enters the picture.

$$\begin{aligned} \hat{b}_\tau(x) - b_\tau(x) &= \mathbb{E} \left[ b_{k\eta}(\hat{X}_{k\eta}) \mid \hat{X}_\tau = x \right] - b_\tau(x) \\ &= \mathbb{E} \left[ b_{k\eta}(\hat{X}_{k\eta}) \mid \hat{X}_\tau = x \right] - \left( b_{k\eta}(x) + \frac{\partial b_\tau(x)}{\partial \tau}(\tau - k\eta) + O((\tau - k\eta)^2) \right) \\ &= \mathbb{E} \left[ b_{k\eta}(\hat{X}_{k\eta}) - b_{k\eta}(\hat{X}_\tau) \mid \hat{X}_\tau = x \right] - \frac{\partial b_\tau(x)}{\partial \tau} \Big|_{\tau=k\eta} (\tau - k\eta) + O((\tau - k\eta)^2) \end{aligned} \quad (54)$$

They prove that the first term in (54) is  $O(\eta)$  and from our additional time-continuity requirement for the drift in Assumption 3, the second term is also  $O(\eta)$ . (Note that  $\tau \in [k\eta, (k+1)\eta]$  thus  $(\tau - k\eta)$  can be at most  $\eta$ ). With this, the rest of the proof from [31] goes through.  $\square$

Next, in Lemma 7 we analyze the sensitivity of the KL divergence to perturbations in its first and second arguments and use Lemma 6 to bound the difference of point-wise KL in discrete and continuous time.

**Lemma 7.** *Assume  $M := \max_x \left| \log\left(\frac{\mathfrak{p}_1(x; s_p)}{\mathfrak{p}_1(x; s_q)}\right) \right|$  is bounded. Then, the point-wise KL between the continuous time processes approximates the point-wise KL between the discrete time processes up to a discretization error  $\epsilon_1(T) = O(1/T)$ :*

$$|D_{\text{KL}}(\mathfrak{p}_1(\cdot; s_p) \| \mathfrak{p}_1(\cdot; s_q)) - D_{\text{KL}}(p_0(\cdot; s_p) \| p_0(\cdot; s_q))| \leq \epsilon_1(T). \quad (55)$$

*Proof.* We first prove a similar relation for generic distributions  $\pi(x), \rho(x)$  and their perturbed versions  $\hat{\pi}(x), \hat{\rho}(x)$ ; Where it is clear from the context, we omit the integration variables. Perturbing the first argument gives us:

$$\begin{aligned} |D_{\text{KL}}(\hat{\pi} \| \rho) - D_{\text{KL}}(\pi \| \rho)| &= \left| \int \hat{\pi}(x) \log \left( \frac{\hat{\pi}(x)}{\rho(x)} \right) - \int \pi(x) \log \left( \frac{\pi(x)}{\rho(x)} \right) + \int (\hat{\pi}(x) \log \pi(x) - \hat{\pi}(x) \log \pi(x)) \right| \\ &= \left| D_{\text{KL}}(\hat{\pi} \| \pi) + \int (\hat{\pi}(x) - \pi(x)) \log \left( \frac{\pi(x)}{\rho(x)} \right) \right| \\ &\leq D_{\text{KL}}(\hat{\pi} \| \pi) + \max_x \left( \left| \log \left( \frac{\pi(x)}{\rho(x)} \right) \right| \right) \int |\hat{\pi}(x) - \pi(x)| \\ &= D_{\text{KL}}(\hat{\pi} \| \pi) + 2 \log M d_{\text{TV}}(\hat{\pi}, \pi) \end{aligned} \quad (56)$$

where  $\log M := \max_x \left| \log\left(\frac{\pi(x)}{\rho(x)}\right) \right|$  and  $d_{\text{TV}}(p, q)$  denotes the total variation distance between distributions  $p$  and  $q$ . Next, perturbing the second argument we get:

$$\begin{aligned} |D_{\text{KL}}(\hat{\pi} \| \hat{\rho}) - D_{\text{KL}}(\hat{\pi} \| \rho)| &= \left| \int \hat{\pi}(x) \log \left( \frac{\hat{\pi}(x)}{\hat{\rho}(x)} \right) - \int \hat{\pi}(x) \log \left( \frac{\hat{\pi}(x)}{\rho(x)} \right) \right| \\ &= - \int \hat{\pi}(x) \log \left( \frac{\hat{\rho}(x)}{\rho(x)} \right) \\ &= - \int \hat{\pi}(x) \log \left( 1 + \frac{\hat{\rho}(x) - \rho(x)}{\rho(x)} \right) \\ &\leq \int \hat{\pi}(x) \frac{\hat{\rho}(x) - \rho(x)}{\rho(x)} \\ &= \int \frac{\hat{\pi}(x)}{\pi(x)} \frac{\pi(x)}{\rho(x)} (\hat{\rho}(x) - \rho(x)) \\ &\leq \max_x \left( \frac{\pi(x)}{\rho(x)} \right) \int |\hat{\rho}(x) - \rho(x)| \\ &= 2M d_{\text{TV}}(\hat{\rho}, \rho). \end{aligned} \quad (57)$$

Using (56) and (57) we get:

$$\begin{aligned}
|D_{\text{KL}}(\hat{\pi} \parallel \hat{\rho}) - D_{\text{KL}}(\pi \parallel \rho)| &\leq |D_{\text{KL}}(\hat{\pi} \parallel \hat{\rho}) - D_{\text{KL}}(\hat{\pi} \parallel \rho)| + |D_{\text{KL}}(\hat{\pi} \parallel \rho) - D_{\text{KL}}(\pi \parallel \rho)| \\
&\leq D_{\text{KL}}(\hat{\pi} \parallel \pi) + 2M d_{\text{TV}}(\hat{\rho}, \rho) + 2 \log M d_{\text{TV}}(\hat{\pi}, \pi) \\
&\leq D_{\text{KL}}(\hat{\pi} \parallel \pi) + 2M \sqrt{\frac{1}{2} D_{\text{KL}}(\hat{\rho} \parallel \rho)} + 2 \log M \sqrt{\frac{1}{2} D_{\text{KL}}(\hat{\pi} \parallel \pi)}
\end{aligned} \tag{58}$$

where in the last line we utilized Pinsker's inequality to bound the TV distance with the square root of the KL divergence. Now we apply (58) to diffusion models,

$$\begin{aligned}
|D_{\text{KL}}(\mathbf{p}_1(\cdot; s_p) \parallel \mathbf{p}_1(\cdot; s_q)) - D_{\text{KL}}(p_0(\cdot; s_p) \parallel p_0(\cdot; s_q))| &\leq D_{\text{KL}}(p_0(\cdot; s_p) \parallel \mathbf{p}_1(\cdot; s_p)) \\
&\quad + 2M \sqrt{\frac{1}{2} D_{\text{KL}}(p_0(\cdot; s_q) \parallel \mathbf{p}_1(\cdot; s_q))} \\
&\quad + 2 \log M \sqrt{\frac{1}{2} D_{\text{KL}}(p_0(\cdot; s_p) \parallel \mathbf{p}_1(\cdot; s_p))}.
\end{aligned} \tag{59}$$

Furthermore, from Lemma 6 by setting  $t = 0$  we know

$$D_{\text{KL}}(p_0(\cdot; s_p) \parallel \mathbf{p}_1(\cdot; s_p)) \leq c/T^2, \quad D_{\text{KL}}(p_0(\cdot; s_q) \parallel \mathbf{p}_1(\cdot; s_q)) \leq c/T^2 \tag{60}$$

Putting together (59) and (60) we get:

$$|D_{\text{KL}}(\mathbf{p}_1(\cdot; s_p) \parallel \mathbf{p}_1(\cdot; s_q)) - D_{\text{KL}}(p_0(\cdot; s_p) \parallel p_0(\cdot; s_q))| \leq \epsilon_1(T) \tag{61}$$

where  $\epsilon_1(T) := c/T^2 + (2M + 2 \log M) \sqrt{c/T^2}$ . The second term dominates therefore  $\epsilon_1(T) = O(1/T)$  which concludes the proof.  $\square$

It remains to characterize the discretization error from approximating the continuous time integral in (39) with a sum over discrete time steps which we now do in Lemma 8.

**Lemma 8.** *Assume  $B_1, B_2$  as defined below are finite:*

$$\begin{aligned}
B_1 &:= \sup_{x, \tau} \|s_p(x, \tau) - s_q(x, \tau)\|_2 \\
B_2 &:= \sup_{x, \tau} \left\| \frac{d}{d\tau} (s_p(x, \tau) - s_q(x, \tau)) \right\|_2
\end{aligned}$$

*Then, the integral from Lemma 5 giving the point-wise KL in continuous time can be approximated with a discrete time sum as follows:*

$$\left| \int_{\tau=0}^1 \tilde{\omega}_\tau \mathbb{E}_{x \sim \mathbf{p}_\tau(\cdot; s_p)} \left[ \|s_p(x, \tau) - s_q(x, \tau)\|_2^2 \right] - \sum_{t=0}^T \frac{1}{T} \tilde{\omega}_{t/T} \mathbb{E}_{x \sim p_t(\cdot; s_p)} \left[ \|s_p(x, t) - s_q(x, t)\|_2^2 \right] \right| \leq \epsilon_2(T) \tag{62}$$

*where the discretization error is  $\epsilon_2(T) = O(1/T)$ .*

*Proof.* There are two sources of error we need to consider. First we bound the error in approximating an integral with a sum:

$$\begin{aligned}
& \left| \int_{\tau=0}^1 \tilde{\omega}_\tau \mathbb{E}_{x \sim \mathfrak{p}_\tau(\cdot; s_p)} \left[ \|s_p(x, \tau) - s_q(x, \tau)\|_2^2 \right] - \sum_{t=0}^T \frac{1}{T} \tilde{\omega}_{t/T} \mathbb{E}_{x \sim \mathfrak{p}_{t/T}(\cdot; s_p)} \left[ \|s_p(x, t) - s_q(x, t)\|_2^2 \right] \right| \\
&= \left| \int_{\tau=0}^1 f(\tau) d\tau - \sum_{t=0}^T f(t/T) \cdot \frac{1}{T} \right| \\
&\leq \frac{1}{T} \sup_{\tau \in [0, 1]} \left| \frac{df}{d\tau} \right|
\end{aligned}$$

where we have defined  $f(\tau) := \tilde{\omega}_\tau \mathbb{E}_{x \sim \mathfrak{p}_\tau(\cdot; s_p)} \left[ \|s_p(x, \tau) - s_q(x, \tau)\|_2^2 \right]$ . We now upper bound the supremum to show that it is finite:

$$\begin{aligned}
\frac{df}{d\tau} &= \frac{d}{d\tau} \left( \int \mathfrak{p}_\tau(x; s_p) \|s_p(x, \tau) - s_q(x, \tau)\|_2^2 dx \right) \\
&= \int \frac{d}{d\tau} (\mathfrak{p}_\tau(x; s_p)) \|s_p(x, \tau) - s_q(x, \tau)\|_2^2 dx + \int \mathfrak{p}_\tau(x; s_p) \frac{d}{d\tau} (\|s_p(x, \tau) - s_q(x, \tau)\|_2^2) dx
\end{aligned} \tag{63}$$

We bound each term in (63) separately. Then the first term in (63) is bounded because  $\frac{d}{d\tau} (\mathfrak{p}_\tau(x; s_p))$  is finite as characterized in Lemma 4.1. The second term in (63) we expand further:

$$\begin{aligned}
& \int \mathfrak{p}_\tau(x; s_p) \frac{d}{d\tau} (\|s_p(x, \tau) - s_q(x, \tau)\|_2^2) dx \\
&= \int 2\mathfrak{p}_\tau(x; s_p) \langle s_p(x, \tau) - s_q(x, \tau), \frac{ds_p(x, \tau)}{d\tau} - \frac{ds_q(x, \tau)}{d\tau} \rangle dx \\
&\leq 2 \sup_{x, \tau} \|s_p(x, \tau) - s_q(x, \tau)\|_2 \left\| \frac{d}{d\tau} (s_p(x, \tau) - s_q(x, \tau)) \right\|_2 \\
&\leq 2B_1 B_2.
\end{aligned}$$

The second source of error is replacing expectation over the continuous time marginal  $\mathfrak{p}_{t/T}(\cdot; s_p)$  with expectation over the discrete time marginal  $p_t(\cdot; s_p)$  which we can bound by using the fact that the two aforementioned marginals are close to each other.

$$\begin{aligned}
& \left| \sum_{t=0}^T \frac{1}{T} \tilde{\omega}_{t/T} \mathbb{E}_{x \sim \mathfrak{p}_{t/T}(\cdot; s_p)} \left[ \|s_p(x, t) - s_q(x, t)\|_2^2 \right] - \sum_{t=0}^T \frac{1}{T} \tilde{\omega}_{t/T} \mathbb{E}_{x \sim p_t(\cdot; s_p)} \left[ \|s_p(x, t) - s_q(x, t)\|_2^2 \right] \right| \\
&\leq \sum_{t=0}^T \frac{1}{T} \tilde{\omega}_{t/T} d_{TV}(p_t(\cdot; s_p), \mathfrak{p}_{t/T}(\cdot; s_p)) \cdot \sup_x \|s_p(x, \tau) - s_q(x, \tau)\|_2^2 \\
&\leq \sum_{t=0}^T \frac{1}{T} \tilde{\omega}_{t/T} \sqrt{\frac{c}{T^2}} \cdot B_1^2 \\
&\leq T \cdot \frac{1}{T} \cdot \sqrt{\frac{c}{T^2}} \cdot B_1^2 \\
&= O\left(\frac{1}{T}\right)
\end{aligned}$$

where we used Lemma 6 to get the last line, which concludes the proof.  $\square$

It remains to combine Lemmas 7, 8 to complete the proof of Lemma 2,

$$D_{\text{KL}}(p_0(\cdot; s_p) \| p_0(\cdot; s_q)) = \sum_{t=0}^T \tilde{\omega}_t \mathbb{E}_{x \sim p_t(\cdot; s_p)} \left[ \|s_p(x, t) - s_q(x, t)\|_2^2 \right] + \epsilon_T \quad (64)$$

where  $|\epsilon_T| \leq \epsilon_1(T) + \epsilon_2(T) = O(1/T)$ . (We slightly abuse notation to denote  $\frac{1}{T} \tilde{\omega}_t$  as  $\tilde{\omega}_t$  in (64) and in the main paper.)

### C.3 Proof of Theorem 1

*Proof.* For any  $\lambda \geq 0$ , the optimal solution  $p^*(\cdot; \lambda)$  is uniquely determined by solving a partial minimization problem,

$$\underset{p \in \mathcal{P}}{\text{minimize}} \ L_{\text{ALI}}(p, \lambda).$$

Application of Donsker and Varadhan's variational formula yields the optimal solution

$$p^*(\cdot; \lambda) \propto q(\cdot) e^{\lambda^\top r(\cdot)}.$$

Since the strong duality holds for Problem (UR-A), its optimal solution is given by  $p^*(\cdot; \lambda)$  evaluated at  $\lambda = \lambda^*$ .

It is straightforward to evaluate the dual function by the definition  $D(\lambda) = L(p^*(\cdot; \lambda), \lambda)$ .  $\square$

### C.4 Proof of Theorem 2

*Proof.* We first consider the constrained alignment (SR-A) in the path space  $\{p_{0:T}(\cdot)\}$ . Since the KL divergence is convex in the path space and the constraints are linear, the strong duality holds in the path space, i.e., there exists a pair  $(p_{0:T}^*(\cdot), \lambda^*)$  such that

$$\bar{P}_{\text{ALI}}^* := D_{\text{KL}}(p_{0:T}^*(\cdot) \| q_{0:T}(\cdot; s_q)) = \bar{D}_{\text{ALI}}(\lambda^*) := \bar{D}_{\text{ALI}}^*.$$

Equivalently,  $(p_{0:T}^*(\cdot), \lambda^*)$  is a saddle point of the Lagrangian  $L_{\text{ALI}}(p_{0:T}(\cdot), \lambda)$ ,

$$L_{\text{ALI}}(p_{0:T}^*(\cdot), \lambda) \leq L_{\text{ALI}}(p_{0:T}^*(\cdot), \lambda^*) \leq L_{\text{ALI}}(p_{0:T}(\cdot), \lambda^*) \text{ for all } p_{0:T}(\cdot) \text{ and } \lambda \geq 0.$$

Since the function class  $\mathcal{S}$  is expressive enough, any path  $p_{0:T}(\cdot)$  can be represented as  $p_{0:T}(\cdot; s_p)$  with some  $s_p \in \mathcal{S}$ ; and vice versa. Thus, we can express  $p_{0:T}^*(\cdot)$  as  $p_{0:T}(\cdot; s_p^*)$  with some  $s_p^* \in \mathcal{S}$ . We also note that the dual functions  $\bar{D}_{\text{ALI}}(\lambda)$  in the path and function spaces are the same. Hence, the dual value for (SR-A) remains to be  $\bar{D}_{\text{ALI}}(\lambda^*)$ . Thus,  $(s_p^*, \lambda^*)$  is a saddle point of the Lagrangian  $\bar{L}_{\text{ALI}}(s_p, \lambda) := L_{\text{ALI}}(p_{0:T}(\cdot; s_p), \lambda)$ ,

$$\bar{L}_{\text{ALI}}(s_p^*, \lambda) \leq \bar{L}_{\text{ALI}}(s_p^*, \lambda^*) \leq \bar{L}_{\text{ALI}}(s_p, \lambda^*) \text{ for all } s_p \in \mathcal{S} \text{ and } \lambda \geq 0.$$

Therefore, the strong duality holds for (SR-A) in the function space  $\mathcal{S}$ .  $\square$

## C.5 Proof of Theorem 3

*Proof.* By the definition,

$$\begin{aligned}
L_{\text{AND}}(p, u; \lambda) &= u + \sum_{i=1}^m \lambda_i (D_{\text{KL}}(p \| q^i) - u) \\
&= u - u\lambda^\top \mathbf{1} + \sum_{i=1}^m (\lambda_i \mathbb{E}_{x \sim p} [\log p(x)] - \lambda_i \mathbb{E}_{x \sim p} [\log q^i(x)]) \\
&= u - u\lambda^\top \mathbf{1} + \sum_{i=1}^m \lambda_i \mathbb{E}_{x \sim p} [\log p(x)] - \mathbb{E}_{x \sim p} \left[ \log \prod_{i=1}^m (q^i(x))^{\lambda_i} \right] \\
&= u - u\lambda^\top \mathbf{1} \\
&\quad + \sum_{i=1}^m \lambda_i \left( \mathbb{E}_{x \sim p} [\log p(x)] - \mathbb{E}_{x \sim p} \left[ \log \prod_{i=1}^m (q^i(x))^{\frac{\lambda_i}{1^\top \lambda}} \right] \right) \\
&= u + \sum_{i=1}^m \lambda_i \left( D_{\text{KL}}(p \| q_{\text{AND}}^{(\lambda)}) - u \right) - \mathbf{1}^\top \lambda \log Z_{\text{AND}}(\lambda).
\end{aligned}$$

By taking  $\lambda = \lambda^*$ , we obtain a primal problem:  $\underset{p \in \mathcal{P}, u \geq 0}{\text{maximize}} L_{\text{AND}}(p, u; \lambda^*)$ , which solves the constrained alignment problem (UR-A) because of the strong duality. By the variational optimality, maximization of  $L_{\text{AND}}(p, u; \lambda^*)$  over  $p$  and  $u$  is at a unique maximizer,

$$p^*(\cdot; \lambda^*) \propto q_{\text{AND}}^{(\lambda^*)}(\cdot)$$

and  $u^* = 0$  if  $1 - \mathbf{1}^\top \lambda^* \geq 0$  and  $u^* = \infty$  otherwise. This gives the optimal model  $p^*(\cdot) = p^*(\cdot; \lambda^*)$ .

Meanwhile, for any  $\lambda \geq 0$ , the primal problem:  $\underset{p \in \mathcal{P}, u \geq 0}{\text{maximize}} L_{\text{AND}}(p, u; \lambda)$  defines the dual function  $D_{\text{AND}}(\lambda)$ . By the variational optimality, maximization of  $L_{\text{AND}}(p, u; \lambda)$  over  $p$  and  $u$  is at a unique maximizer,

$$p^*(\cdot; \lambda, \mu) \propto q_{\text{AND}}^{(\lambda)}(\cdot)$$

and  $u^*(\lambda) = 0$  if  $1 - \mathbf{1}^\top \lambda \geq 0$  and  $u^*(\lambda) = \infty$  otherwise. This defines the dual function,

$$\begin{aligned}
D_{\text{AND}}(\lambda) &= L_{\text{AND}}(p^*(\cdot; \lambda), u^*(\lambda); \lambda) \\
&= u^*(\lambda) + \sum_{i=1}^m \lambda_i \left( D_{\text{KL}}(p^*(\cdot; \lambda) \| q_{\text{AND}}^{(\lambda)}(\cdot)) - u^*(\lambda) \right) - \mathbf{1}^\top \lambda \log Z_{\text{AND}}(\lambda) \\
&= (1 - \mathbf{1}^\top \lambda) u^*(\lambda) - \mathbf{1}^\top \lambda \log Z_{\text{AND}}(\lambda)
\end{aligned}$$

which completes the proof by following the definition of the dual problem and the dual constraint  $\mathbf{1}^\top \lambda \leq 1$ .  $\square$

## C.6 Proof of Theorem 4

*Proof.* Similar to the proof of Theorem 2, we can establish a saddle point condition for the Lagrangian  $\bar{L}_{\text{AND}}(s_p, u, \lambda)$  by leveraging the expressiveness of the function class  $\mathcal{S}$  which represents the path space  $\{p_{0:T}(\cdot)\}$ . As the proof follows similar steps, we omit the detail.  $\square$

## C.7 Proof of Lemma 3

*Proof.* From section C.5, we recall:

$$L_{\text{AND}}(p, u; \lambda) = u + \sum_{i=1}^m \lambda_i \left( D_{\text{KL}}(p \parallel q_{\text{AND}}^{(\lambda)}) - u \right) - \mathbf{1}^\top \lambda \log Z_{\text{AND}}(\lambda). \quad (65)$$

Since in the diffusion formulation of the problem (SR-A) we have  $p = p_0(x_0; s)$ ,  $q^i = p_0(x_0; s^i)$ , we can derive similarly to (65) that:

$$L_{\text{AND}}(p_0(\cdot; s), u; \lambda) = u + \sum_{i=1}^m \lambda_i \left( D_{\text{KL}}(p_0(\cdot; s) \parallel q_{\text{AND},0}^{(\lambda)}(\cdot)) - u \right) - \mathbf{1}^\top \lambda \log Z_{\text{AND}}(\lambda). \quad (66)$$

Since minimizing over  $u$  would trivially give  $\min_u L_{\text{AND}}(p, u; \lambda) = -\infty$  unless  $\lambda^\top \mathbf{1} = 1$ , we consider the Lagrangian in the non-trivial case where  $\lambda^\top \mathbf{1} = 1$ . Then we have:

$$L_{\text{AND}}(p(\cdot; s); \lambda) = L_{\text{AND}}(s, \lambda) = D_{\text{KL}}(p_0(\cdot; s) \parallel q_{\text{AND},0}^{(\lambda)}) - \log Z_{\text{AND}}(\lambda). \quad (67)$$

The second term  $\log Z_{\text{AND}}(\lambda)$  does not depend on  $s$ , thus it suffices to minimize  $D_{\text{KL}}(p_0(\cdot; s) \parallel q_{\text{AND},0}^{(\lambda)})$  to find the Lagrangian minimizer which we call  $s^{(\lambda)}$ . The KL is minimized when  $p_0(\cdot; s^{(\lambda)}) = q_{\text{AND},0}^{(\lambda)}$ . If we have access to samples from  $q_{\text{AND},0}^{(\lambda)}$ , we can fit  $s$  to  $q_{\text{AND},0}^{(\lambda)}$  by optimizing the Denoising score matching objective similar to Equation (1) in [41]:

$$L_{\text{sm}}(s, \lambda) = \sum_{t=0}^T \omega_t \mathbb{E}_{x_0 \sim q_{\text{AND}}^{(\lambda)}(\cdot)} \mathbb{E}_{x_t \sim q(x_t|x_0)} \left[ \|s(x, t) - \nabla \log q(x_t|x_0)\|^2 \right] \quad (68)$$

From [41] we know that given sufficient data and predictor capacity of  $s$  we have  $\operatorname{argmin}_s L_{\text{sm}}(s, \lambda) \simeq q_{\text{AND},0}^{(\lambda)}$ .  $\square$

## D Composition with Forward KL Divergences

We start with the constrained problem formulation using forward KL divergence (UF-C) which we rewrite here:

$$\begin{aligned} & \underset{u \in \mathbb{R}, p \in \mathcal{P}}{\text{minimize}} \quad u \\ & \text{subject to} \quad D_{\text{KL}}(q^i \| p) \leq u \quad \text{for } i = 1, \dots, m. \end{aligned} \quad (69)$$

In the case of diffusion models, the KL divergence in (69) becomes the forward path-wise KL between the processes:

$$\begin{aligned} & \underset{u \in \mathbb{R}, p \in \mathcal{P}}{\text{minimize}} \quad u \\ & \text{subject to} \quad D_{\text{KL}}(q_{0:T}^i(\cdot) \| p_{0:T}(\cdot; s)) \leq u \quad \text{for } i = 1, \dots, m. \end{aligned} \quad (70)$$

It is important to note here that using the forward KL as a constraint makes sense when  $q^i$  represent forward diffusion processes obtained by adding noise to samples from some dataset. We can also solve this forward KL constrained problem to compose multiple models; In that case we treat samples generated by each model as a separate dataset with underlying distribution  $q_0^i(x_0)$ .

In summary, the two key differences of Problem (70) to Problem (UR-A) are: (i) The closeness of a model  $p$  to a pretrained model  $q^i$  is measured by the forward KL divergence  $D_{\text{KL}}(q^i \| p)$ , instead of the reverse KL divergence  $D_{\text{KL}}(p \| q^i)$ ; (ii) The distributions  $\{q^i\}_{i=1}^m$  can be the distributions underlying  $m$  datasets, not necessarily  $m$  pretrained models.

Regardless of whether the  $q^i$  represent pre-trained models or datasets, evaluating  $D_{\text{KL}}(q_{0:T}^i(\cdot) \| p_{0:T}(\cdot; s))$  is intractable since it requires knowing  $q_{0:T}^i(\cdot)$  which in turn requires knowing  $q_0^i(\cdot)$  exactly. To get around this issue we formulate a closely related problem to (70) by replacing the KL with the Evidence Lower Bound (Elbo):

$$\begin{aligned} & \underset{u \in \mathbb{R}, p \in \mathcal{P}}{\text{minimize}} \quad u \\ & \text{subject to} \quad \text{Elbo}(q_{0:T}^i; p_{0:T}) \leq u \quad \text{for } i = 1, \dots, m \end{aligned} \quad (71)$$

where the Elbo is defined as

$$\text{Elbo}(q_{0:T}; p_{0:T}) := \mathbb{E}_{x_0 \sim q_0} \mathbb{E}_{q(x_{1:T} | x_0)} \log \frac{p_{0:T}(x_{0:T})}{q(x_{1:T} | x_0)}. \quad (72)$$

We note that the typical approach to train a diffusion model is minimizing the Elbo. Furthermore, minimizing  $\text{Elbo}(q_{0:T}; p_{0:T})$  over  $p$  is equivalent to minimizing the KL divergence  $D_{\text{KL}}(q_{0:T}^i(\cdot) \| p_{0:T}(\cdot; s))$  since they only differ by a constant that does not depend on  $p$ . (see [21] for more details on this)

For a given  $\lambda$ , we define a weighted mixture of distributions as

$$q_{\text{mix}}^{(\lambda)}(\cdot) = \sum_{i=1}^m \frac{\lambda_i}{\lambda^T 1} q^i(\cdot), \quad (73)$$

and we denote by  $H(q)$  the differential entropy of a given distribution  $q$ ,

$$H(q) := -\mathbb{E}_{x \sim q} [\log q(x)] \quad (74)$$

**Theorem 5.** *Problem (71) is equivalent to the following unconstrained problem:*

$$\underset{p \in \mathcal{P}}{\text{minimize}} \ D_{\text{KL}}(q_{\text{mix}}^{(\lambda^*)} \parallel p) \quad (75a)$$

where  $\lambda^*$  is the optimal dual variable given by  $\lambda^* = \text{argmax}_{\lambda \geq 0} D(\lambda)$ . The dual function has the explicit form,  $D(\lambda) = H(q_{\text{mix}}^{(\lambda)})$ . Furthermore, the optimal solution of (7) is given by

$$p^* = q_{\text{mix}}^{(\lambda^*)}. \quad (75b)$$

Unlike the reverse KL case, here we can characterize the optimal dual multipliers, and the optimal solution further; Note that the optimal dual multiplier  $\lambda^* = \text{argmax}_{\lambda \geq 0} D(\lambda) = \text{argmax}_{\lambda \geq 0} H(q_{\text{mix}}(\cdot; \lambda^*))$  is one that maximizes the differential entropy  $H(\cdot)$  of the distribution of the corresponding mixture. This implies that the optimal solution is the most diverse mixture of the individual distributions.

There are many potential use cases where we may want to compose distributions that don't overlap in their supports; For example when combining distributions of multiple dissimilar classes of a dataset. The following characterizes the optimal solution in such settings.

**Corollary 1.** *For the special case where the distributions  $q^i$  all have disjoint supports, the optimal dual multiplier  $\lambda^*$  of Problem (71) can be characterized explicitly as*

$$\lambda_i^* = \frac{e^{H(q^i)}}{\sum_{j=1}^m e^{H(q^j)}}.$$

## E Algorithm Details

### E.1 Alignment

Recall from Section 3.1 that the algorithm consists of two alternating steps:

**Primal minimization:** At iteration  $n$ , we obtain a new model  $s^{(n+1)}$  via a Lagrangian maximization,

$$s^{(n+1)} \in \underset{s \in \mathcal{S}}{\text{argmin}} \bar{L}_{\text{ALI}}(s_p, \lambda^{(n)}).$$

**Dual maximization:** Then, we use the model  $s^{(n+1)}$  to estimate the constraint violation  $\mathbb{E}_{x_0}[r(x_0)] - b$ , denoted as  $r(s^{(n+1)}) - b$ , and perform a dual sub-gradient ascent step,

$$\lambda^{(n+1)} = \left[ \lambda^{(n)} + \eta \left( r(s^{(n+1)}) - b \right) \right]_+.$$

In practice we replace minimization over  $\mathcal{S}$  with minimization over a parametrized family of functions  $\mathcal{S}_\theta$ . The full algorithm is detailed in Algorithm 1.

---

**Algorithm 1** Primal-Dual Algorithm for Reward Alignment of Diffusion Models

---

- 1: **Input:** total diffusion steps  $T$ , diffusion parameter  $\alpha_t$ , total dual iterations  $H$ , number of primal steps per dual update  $N$ , dual step size  $\eta_d$ , primal step size  $\eta_p$ , initial model parameters  $\theta(0)$ .
- 2: **Initialize:**  $\lambda(1) = 1/m$ .
- 3: **for**  $h = 1, \dots, H$  **do**
- 4:     Initialize  $\theta_1 = \theta(h-1)$
- 5:     **for**  $n = 1, \dots, N$  **do**
- 6:         Take a primal gradient descent step

$$\theta_{n+1} = \theta_n - \eta_p \nabla_{\theta} \bar{L}_{\text{ALI}}(\theta, \lambda^{(n)}) \quad (76)$$

- 7:     **end for**
- 8:     Set the value of the parameters to be used for the next dual update:  $\theta(h) = \theta_{N+1}$ .
- 9:     Update dual multipliers for  $i = 1, \dots, m$ :

$$\lambda_i(h+1) = [\lambda_i(h) + \eta_d (\mathbb{E}_{x_0 \sim p_0(\cdot; s_{\theta})} [r_i(x_0)] - b_i)]_+ \quad (77)$$

- 10: **end for**
- 

We now discuss the practicality of the primal gradient descent step (76) regarding the Lagrangian function,

$$\bar{L}_{\text{ALI}}(\theta, \lambda) = D_{\text{KL}}(p_{0:T}(\cdot; s_{\theta}) \| q_{0:T}(\cdot; s_q)) - \sum_i \lambda_i (\mathbb{E}_{x_0 \sim p_0(\cdot; s_{\theta})} [r_i(x_0)] - b_i) \quad (78)$$

To derive the gradient of  $\bar{L}_{\text{ALI}}(\theta, \lambda)$ , we first take the derivative of the expected reward terms by noting that the expectation is taken over a distribution that depends on the optimization variable  $\theta$ . We can use the following result (Lemma 4.1 from [16]) to take the gradient inside the expectation.

**Lemma 9.** *If  $p_{\theta}(x_{0:T})r(x_0)$  and  $\nabla_{\theta}p_{\theta}(x_{0:T})r(x_0)$  are continuous functions of  $\theta$ , then we can write the gradient of the reward function as*

$$\nabla_{\theta} \mathbb{E}_{x_0 \sim p_0(\cdot; s_{\theta})} [r(x_0)] = \mathbb{E}_{x_{0:T} \sim p_{0:T}(\cdot; s_{\theta})} \left[ r(x_0) \sum_{t=1}^T \nabla_{\theta} \log p(x_{t-1} | x_t; s_{\theta}) \right].$$

For the gradient of the KL divergence, we have

$$\begin{aligned} & \nabla_{\theta} D_{\text{KL}}(p_{0:T}(\cdot; s_{\theta}) \| q_{0:T}(\cdot; s_q)) \\ &= \nabla_{\theta} \left( \sum_{t=1}^T \mathbb{E}_{x_t \sim p_t(\cdot; s_{\theta})} \left[ \frac{1}{2\sigma_t^2} \|s_{\theta}(x_t, t) - s_q(x_t, t)\|^2 \right] \right) \\ &= \nabla_{\theta} \left( \sum_{t=1}^T \mathbb{E}_{x_t \sim p_t(\cdot; s_{\theta})} [D_{\text{KL}}(p(x_{t-1} | x_t; s_{\theta}) \| p(x_{t-1} | x_t; s_q))] \right) \\ &= \sum_{t=1}^T \mathbb{E}_{x_t \sim p_t(\cdot; s_{\theta})} [\nabla_{\theta} D_{\text{KL}}(p(x_{t-1} | x_t; s_{\theta}) \| p(x_{t-1} | x_t; s_q))] \\ &+ \sum_{t=1}^T \mathbb{E}_{x_t \sim p_t(\cdot; s_{\theta})} \left[ \sum_{t' > t}^T \nabla_{\theta} \log p(x_{t'-1} | x_{t'}; s_{\theta}) D_{\text{KL}}(p(x_{t-1} | x_t; s_{\theta}) \| p(x_{t-1} | x_t; s_q)) \right]. \end{aligned}$$

The second term we ignore in practice for simplicity without hurting performance. See [16, Appendix A.3] for the derivation.

## E.2 Composition

For composition, we take a similar approach to Algorithm 1. Recall from Lemma 3 that the Lagrangian minimizer for the constrained composition problem can be found by minimizing:

$$\widehat{L}_{\text{AND}}(\theta, \lambda) := \sum_{t=0}^T \omega_t \mathbb{E}_{x_0 \sim q_{\text{AND}}^{(\lambda)}(\cdot)} \mathbb{E}_{x_t \sim q(x_t|x_0)} \left[ \|s_\theta(x, t) - \nabla \log q(x_t|x_0)\|^2 \right]$$

Thus, we detail the algorithm for composition in Algorithm 2.

---

### Algorithm 2 Primal-Dual Algorithm for Product Composition (AND) of Diffusion Models

---

- 1: **Input:** total diffusion steps  $T$ , diffusion parameter  $\alpha_t$ , total dual iterations  $H$ , number of primal steps per dual update  $N$ , dual step size  $\eta_d$ , primal step size  $\eta_p$ , initial model parameters  $\theta(0)$ .
- 2: **Initialize:**  $\lambda(1) = 1/m$ .
- 3: **for**  $h = 1, \dots, H$  **do**
- 4:     Initialize  $\theta_1 = \theta(h-1)$
- 5:     **for**  $n = 1, \dots, N$  **do**
- 6:         Take a primal gradient descent step
- 7:     **end for**
- 8:     Set the value of the parameters to be used for the next dual update:  $\theta(h) = \theta_{N+1}$ .
- 9:     Update dual multipliers for  $i = 1, \dots, m$ :

$$\tilde{\lambda}_i(h+1) = \lambda_i(h) + \eta_d D_{\text{KL}}(p_0(\cdot; s_{\theta(h)}) \| p_0(\cdot; s^i)) \quad (79)$$

- 10:      $\lambda(h+1) = \text{proj}(\tilde{\lambda}(h+1))$ , where  $\text{proj}(y)$  projects its input onto the simplex  $\lambda^T 1 = 1$ .
  - 11: **end for**
- 

The projection of the dual multipliers vector at the end is because we are maximizing the Dual function and as seen in the proof of Theorem 3 this requires that  $\lambda^\top 1 = 1$ .

Note that implicit in Algorithm 2 is the fact that for minimizing the Lagrangian  $\widehat{L}_{\text{AND}}(\theta, \lambda)$  we need samples from the weighted product distribution  $q_{\text{AND}}^{(\lambda)}(\cdot)$ . We do this using the Annealed MCMC sampling algorithm proposed in [14].

**Skipping the Primal.** As mentioned in Section 5, Annealed MCMC sampling and the minimization of the Lagrangian  $\widehat{L}_{\text{AND}}(\theta, \lambda)$  at each primal step to match the true score  $\nabla \log q_{\text{AND}}^\lambda$  are both difficult and computationally costly. This is why for the settings other than the Low-Dimensional setting discussed in Appendix F.1 we propose Algorithm 3 that skips the primal step entirely.

We achieve this by using the surrogate product score (rather than the true score) for computing the point-wise KL needed for the dual updates. The difference between the two is also discussed in [14].

$$\text{true score: } \nabla \log q_{\text{AND},t}^{(\lambda)}(x_t) = \nabla \log \left( \int \sum_i (q_0(x_0))^{\lambda_i} q(x_t|x_0) dx_0 \right) \quad (81)$$

$$\text{surrogate score: } \nabla \log \hat{q}_{\text{AND},t}^{(\lambda)}(x_t) = \sum_i \lambda_i \nabla \log \left( \int q_0(x_0) q(x_t|x_0) dx_0 \right) \quad (82)$$

---

**Algorithm 3** Dual-Only Algorithm for Product Composition (AND) of Diffusion Models

---

- 1: **Input:** total diffusion steps  $T$ , diffusion parameter  $\alpha_t$ , total dual iterations  $H$ , dual step size  $\eta_d$ .
  - 2: **Initialize:**  $\lambda(1) = 1/m$ .
  - 3: **for**  $h = 1, \dots, H$  **do**
  - 4:     Update dual multipliers for  $i = 1, \dots, m$ :
- $$\tilde{\lambda}_i(h+1) = \lambda_i(h) + \eta_d D_{\text{KL}} \left( \hat{q}_{\text{AND},0}^{(\lambda(h))}(\cdot) \parallel p_0(\cdot; s^i) \right) \quad (83)$$
- 5:      $\lambda(h+1) = \text{proj} \left( \tilde{\lambda}(h+1) \right)$ , where  $\text{proj}(y)$  projects its input onto the simplex  $\lambda^T 1 = 1$ .
  - 6: **end for**
- 

For a given  $\lambda$ , the surrogate score can be easily computed:

$$\begin{aligned} \nabla \log \hat{q}_{\text{AND},t}^{(\lambda)}(x_t) &= \sum_i \lambda_i \nabla \log \left( \int q_0(x_0) q(x_t|x_0) dx_0 \right) \\ &= \sum_i \lambda_i \nabla \log p_t(x_t; s^i) \end{aligned}$$

and thus we can use Lemma 2 to compute the point-wise KLs needed for the dual update. As for the samples needed from the true product distribution, we also replace them with samples obtained by running DDIM using the surrogate score.

## F More Experiments and Experimental Details

### F.1 Low-dimensional synthetic experiments

For illustrating the difference between the constrained and unconstrained approach visually, we set up experiments where the generated samples are in  $\mathbb{R}^2$ . For the score predictor we used the same ResNet architecture as used in [14].

**Product composition (AND).** Unlike the image experiments, in this low-dimensional setting we used Algorithm 2 for product composition. See Figure 1 for visualization of the resulting distributions.

**Mixture composition (OR).** For this experiment we used the same Algorithm as the one used in [21] for mixture of distributions. The only modification is doing an additional dual multiplier projection step similar to the last step of the product composition Algorithm 2. See Figure 2 for visualization of the resulting distributions.

### F.2 Reward product composition (section 5.2 (I))

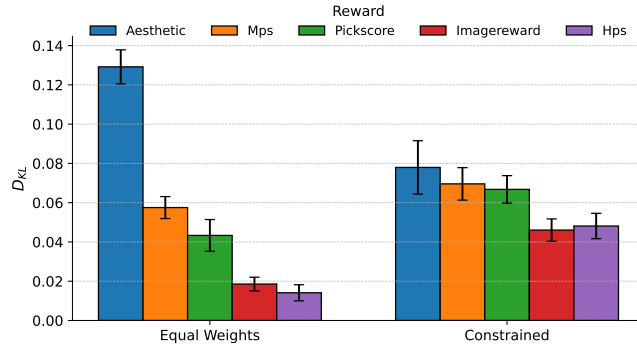


Figure 7: KL divergence for the product composition of 5 adapters pre-trained with different rewards. Error bars denote the standard deviation computed across 8 text prompts each with four samples.

**Implementation details and hyperparameters.** We finetuned the model using the Alignprop [33] official implementation <sup>4</sup> for each individual reward using the hyperparameters reported in Table 2. We then composed the trained adapters running dual ascent using the surrogate score as described in section E.2. We use the average of scores (denoted as “Equal weights”) as a baseline. Hyperparameters are described in Table 3. The reward values reported in Figure 4 were normalised so that 0% corresponds to the reward obtained by the pre-trained model, and 100% the reward obtained by the model fine-tuned solely on the corresponding reward.

**Additional results.** As shown in Figure 7, equal weighting leads to disparate KL’s across adapters – in particular high KL with respect to the adapter trained with the “aesthetic” reward – while our constrained approach effectively reduces the worst case KL, equalizing divergences across adapters. Figure 11 shows images sampled from these two compositions exhibit different characteristics, with our

<sup>4</sup><https://github.com/mihi1998/AlignProp>

constrained approach producing smoother backgrounds, shallower depth of field and more painting-like images.

Hyperparameter	Value
Batch size	64
Samples per epoch	128
Epochs	10
Sampling steps	50
Backpropagation sampling	Gaussian
KL penalty	0.1
Learning rate	$1 \times 10^{-3}$
LoRA rank	4

Table 2: Hyperparameters used to finetune models using individual rewards.

Hyperparameter	Value
Base model	<code>runwayml/stable-diffusion-v1-5</code>
Prompts	<code>{"cheetah", "snail", "hippopotamus", "crocodile", "lobster", "octopus"}</code>
Resolution	512
Batch size	4
Dual steps	5
Dual learning rate	1.0
Sampling steps	25
Guidance scale	5.0
Rewards	<code>aesthetic, hps, pickscore, imagereward, mps</code>

Table 3: Hyperparameters for product composition of models finetuned with different rewards.

### F.3 Concept composition (Section 5.2 (II))

We present additional results for concept composition using three different concepts (as opposed to just 2 in the main paper and in [38]) As seen in table 5, our approach retains a clear advantage in both CLIP and BLIP scores. See Figure 6 for examples of images generated using each method. Images with the constrained method typically do a better job of representing all of the individual concepts.

The role of guidance scale here is important in the results. As described in the main paper, the two (or more) models being combined here are a pretrained model, in this case Stable Diffusion, conditioned on different text prompts. Thus the three scores of interest in the algorithm are the following:

$$\begin{aligned}
s_1(x, t) &= \nabla \log(p_t(x)p_t(c_1|x)^w) \\
&= \nabla \log p_t(x) + w(\nabla \log p_t(x, c_1) - \nabla \log p_t(x)) \\
s_2(x, t) &= \nabla \log(p_t(x)p_t(c_2|x)^w) \\
&= \nabla \log p_t(x) + w(\nabla \log p_t(x, c_2) - \nabla \log p_t(x)) \\
s_{(\lambda)}(x, t) &= \nabla \log \left( p_t(x)(p_t(c_1|x)^\lambda p_t(c_2|x)^{1-\lambda})^{w'} \right) \\
&= \nabla \log p_t(x) + \lambda w'(\nabla \log p_t(x, c_1) - \nabla \log p_t(x)) \\
&\quad + (1 - \lambda) w'(\nabla \log p_t(x, c_2) - \nabla \log p_t(x))
\end{aligned} \tag{84}$$

Above,  $s_1$  and  $s_2$  represent the scores of the pre-trained model conditioned on prompts  $c_1$  and  $c_2$  using classifier guidance with weight  $w$ . Next,  $s_{(\lambda)}$  represents the surrogate score for the combined model with guidance weight  $w'$ . (see E.2 for details on the surrogate score).

We then use Algorithm 3 to find the optimal dual multiplier  $\lambda^*$  such that the KL divergences of the model with the surrogate score to each individual model (with scores  $s_i$ ) are equal. Recall that the point-wise KL is computed using (4). Since as seen in (84),  $\nabla \log p_t(x)$  appears in all the scores, it cancels out in computing the KLS. Thus the optimal  $\lambda^*$  depends on the ratio  $\kappa := \frac{w}{w'}$ .

We now argue that if the ratio  $\kappa$  is very small, the dependence of  $\lambda^*$  on this hyper-parameter will be negligible. Furthermore, the solution will have a useful property that we will discuss next. For conciseness we name  $g_i := \nabla \log p_t(x, c_i) - \nabla \log p_t(x)$ .

Consider only the expectation terms in (4). For the KLS to be equal, these terms have to be equal,

$$\begin{aligned}
D_{\text{KL}}(p_0(\cdot; s_{(\lambda^*)}) \| p_0(\cdot; s_1)) &= D_{\text{KL}}(p_0(\cdot; s_{(\lambda^*)}) \| p_0(\cdot; s_2)) \\
\Rightarrow \|s_{(\lambda^*)}(x, t) - s_1(x, t)\|_2^2 &= \|s_{(\lambda^*)}(x, t) - s_2(x, t)\|_2^2 \\
\Rightarrow \|\lambda^* w' g_1 + w'(1 - \lambda^*) g_2 - w g_1\|_2^2 &= \|\lambda^* w' g_1 + w'(1 - \lambda^*) g_2 - w g_2\|_2^2 \\
\Rightarrow \|\lambda^* g_1 + (1 - \lambda^*) g_2 - \kappa g_1\|_2^2 &= \|\lambda^* g_1 + (1 - \lambda^*) g_2 - \kappa g_2\|_2^2
\end{aligned}$$

Now we assume  $\kappa \ll 1$  and ignore terms that are  $O(\kappa^2)$  or higher,

$$\Rightarrow \kappa \langle \lambda^* g_1 + (1 - \lambda^*) g_2, g_1 \rangle = \kappa \langle \lambda^* g_1 + (1 - \lambda^*) g_2, g_2 \rangle$$

This means the projection of the optimal guidance direction given by  $(\lambda^* g_1 + (1 - \lambda^*) g_2)$  onto each of the guidance directions of for the individual concepts i.e.  $g_i = \nabla \log p_t(x, c_i) - \nabla \log p_t(x)$ , is equal.

Intuitively, the model guided with the optimal  $\lambda^*$  is guided equally towards each individual concept  $c_i$  in terms of log-likelihood which is desirable. This is reflected in the improved minimum CLIP and BLIP scores as reported in tables 1, 5. The hyperparameters used for concept composition can be found in 4.

Hyperparameter	Value
Batch size	2
Epochs	50
DDIM inference steps	20
Dual learning rate	0.050
Guidance weight ratio ( $\kappa$ )	0.02

Table 4: Hyperparameters used for Concept Composition Using Algorithm 3

	Min. CLIP ( $\uparrow$ )	Min. BLIP ( $\uparrow$ )
Combined Prompting	21.52	0.206
Equal Weights	22.18	0.203
Constrained (Ours)	<b>22.45</b>	<b>0.221</b>

Table 5: Comparing constrained approach to baselines on minimum CLIP and BLIP scores. The scores are averaged over 50 different prompt triplets sampled from a list of simple prompts.

#### F.4 Alignment experiments

**Reward normalization.** In practice, setting constraint levels for multiple rewards that are both feasible and sufficiently strict to enforce the desired behavior is challenging. Different rewards exhibit widely varying scales. This is illustrated in Table 6, which shows the mean and standard deviation of reward values for the pre-trained model. This issue can be exacerbated by the unknown interdependencies among constraints and the lack of prior knowledge about their relative difficulty or sensitivity.

In order to tackle this, we propose normalizing rewards using the pre-trained model statistics as a simple yet effective heuristic. This normalization facilitates the setting of constraint levels, enables direct comparisons across rewards and enhances interpretability. In all of our experiments, we apply this normalization before enforcing constraints. Explicitly, we set

$$\tilde{r} = \frac{r - \hat{\mu}_{\text{pre}}}{\hat{\sigma}_{\text{pre}}} \quad (85)$$

where  $r$  denotes the original reward and  $\hat{\mu}_{\text{pre}}, \hat{\sigma}_{\text{pre}}$  the sample mean and standard deviation of the reward for the pre-trained model. We find that, with this simple transformation, setting equal constraint levels can yield satisfactory results while forgoing extensive hyperparameter tuning.

Reward	Mean	Std
Aesthetic	5.1488	0.4390
HPS	0.2669	0.0057
MPS	5.2365	3.5449
PickScore	21.1547	0.6551
Local Contrast	0.0086	0.0032
Saturation	0.1060	0.0706

Table 6: Mean and standard deviation of reward values for the pre-trained model.

### I. MPS + local contrast, saturation.

In this experiment, we augment a standard alignment loss—trained on user preferences—with two differentiable rewards that control specific image characteristics: local contrast and saturation. These rewards are computationally inexpensive to evaluate and offer direct interpretability in terms of their visual effect on the generated images. In addition, the unconstrained maximization of these features would lead to undesirable generations. other potentially useful rewards not explored in this work are brightness, chroma energy, edge strength, white balancing and histogram matching.

**Local contrast reward.** In order to prevent images with excessive sharpness, we minimize the “local contrast”, which we define as the mean absolute difference between the luminance of the image and a low-pass filtered version. Explicitly, let  $Y$  denote the luminance, computed as  $Y = 0.2126R + 0.7152G + 0.0722B$ , and  $G_\sigma * Y$  the luminance blurred with a Gaussian kernel of standard deviation  $\sigma = 1.0$ . We minimize the average per pixel difference by maximizing the reward

$$r_C = -\frac{1}{HW} \sum_{i,j} \left| Y_{ij} - (G_\sigma * Y)_{ij} \right|,$$

where  $H, W$  denote image dimensions.

**Saturation reward.** To discourage overly saturated images, we simply penalize saturation, which we compute from  $R, G, B$  pixel values as

$$r_S = -\frac{1}{HW} \sum_{i,j} \frac{\max_{c \in \{R, G, B\}} x_{i,j}^{(c)} - \min_{c \in \{R, G, B\}} x_{i,j}^{(c)}}{\max_{c \in \{R, G, B\}} x_{i,j}^{(c)} + \varepsilon},$$

where  $\varepsilon = 1 \times 10^{-8}$  is a small constant added for numerical stability.

**Implementation details and hyperparameters.** We implemented our primal-dual alignment approach (Algorithm 1) in the Alignprop framework. Following their experimental setting, we use different animal prompts for training and evaluation. Hyperparameters are detailed in Table 7.

Hyperparameter	Value
Base model	runwayml/stable-diffusion-v1-5
Sampling steps	15
Dual learning rate	0.05
Batch size (effective)	$4 \times 16 = 64$
Samples per epoch	128
Epochs	20
KL penalty	0.1
LoRA rank	4
	MPS: 0.5
Constraint level	Saturation: 0.5 Local contrast: 0.25
Equal weights	0.2

Table 7: Hyperparameters for reward alignment with contrast and saturation constraints. Constraint levels correspond to normalised rewards.

**Additional results.** We include images sampled from the constrained model in Figure 13 for hps and aesthetic reward functions. Samples from a model trained with an equally weighted model are included for comparison. Constraints prevent overfitting to the saturation and smoothness penalties.

## II. Multiple aesthetic constraints

**Implementation details and hyperparameters.** We modified the Alignprop framework to accomodate Algorithm 1. Following their setup, we use text conditioning on prompts of simple animals, using separate sets for training and evaluation. In this setting, due to the high variability of rewards throughout training, utilized an exponential moving average to reduce the variance in slack estimates (and hence dual subgradients) [39]. Hyperparameters are detailed in Table 8.

Hyperparameter	Value
Base model	<code>runwayml/stable-diffusion-v1-5</code>
Sampling steps	15
Dual learning rate	0.05
Batch size (effective)	$4 \times 16 = 64$
Samples per epoch	128
Epochs	25
KL penalty	0.1
LoRA rank	4
	MPS: 0.5
	HPS: 0.5
Constraint level	Aesthetic: 0.5 Pickscore : 0.5
Equal weights	0.2 <code>{"cat", "dog", "horse", "monkey", "rabbit", "zebra", "spider", "bird", "sheep", "deer", "cow", "goat", "lion", "tiger", "bear", "raccoon", "fox", "wolf", "lizard", "beetle", "ant", "butterfly", "fish", "shark", "whale", "dolphin", "squirrel", "mouse", "rat", "snake", "turtle", "frog", "chicken", "duck", "goose", "bee", "pig", "turkey", "fly", "llama", "camel", "bat", "gorilla", "hedgehog", "kangaroo"}</code>
Training Prompts	<code>{"cheetah", "snail", "hippopotamus", "crocodile", "lobster", "octopus"}</code>
Evaluation Prompts	

Table 8: Hyperparameters for reward alignment with multiple rewards. Constraint levels correspond to normalised rewards.

**Additional results.** We include two images per method and prompt in Figure 12. These are sampled from the same latents for both models.

## F.5 Sensitivity to Constraint Thresholds

What we observed by varying the reward constraint thresholds in our experiments was that for thresholds up to 1.0 (meaning  $\text{mean} + 1.0 * \text{std}$  for each reward) the model was typically able to satisfy the constraints with minimal violation. Another trend that we observed was that increasing thresholds usually leads to constraints that are harder to satisfy leading to higher Lagrange multipliers and resulting in higher KL to the pre-trained model.

An advantage of our constrained approach is that Lagrange multipliers give information about the sensitivity of the objective with respect to relaxing the constraints i.e. if the multiplier for a certain reward ends up being much higher than the rest it means that constraint is particularly harder to satisfy.

Consequently, even slightly relaxing the threshold for the corresponding reward can lead to much smaller KL objective. See Tables 9 and 10 for the results of varying thresholds for Alignment experiment with MPS and Pickscore rewards respectively. (in both cases we also have saturation and contrast constraints.)

Table 9: MPS reward alignment with saturation and contrast constraints, for varying thresholds.

Constraint	Threshold	Slack	Dual Variable	$D_{KL}$
contrast	0.250	-0.245	0.282	0.177
contrast	0.500	-0.985	0.000	0.296
contrast	1.000	-0.381	0.000	0.332
saturation	0.250	-0.126	0.081	0.177
saturation	0.500	0.060	0.006	0.296
saturation	1.000	0.052	1.195	0.332

Table 10: Pickscore reward alignment with saturation and contrast constraints, for varying thresholds.

Constraint	Threshold	Slack	Dual Variable	$D_{KL}$
contrast	0.250	-0.684	0.000	0.136
contrast	0.500	-1.011	0.000	0.109
contrast	1.000	0.661	0.192	0.293
saturation	0.250	-0.025	0.014	0.136
saturation	0.500	-0.060	0.000	0.109
saturation	1.000	0.062	1.020	0.293

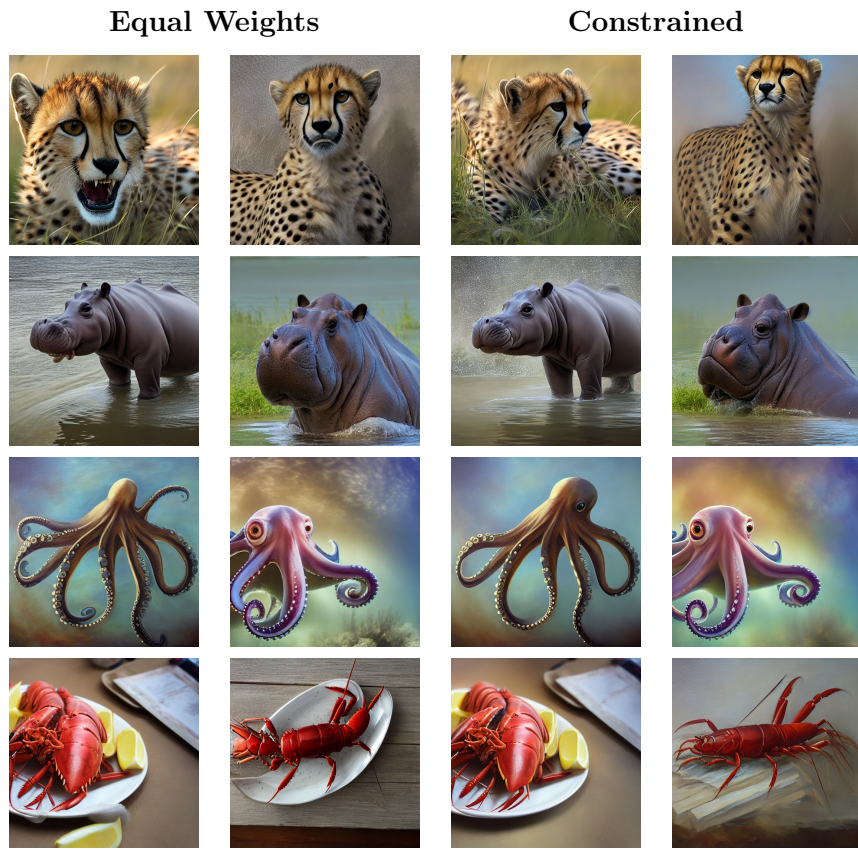


Table 11: Images sampled from the same latents for the product of adapters using the equal weights and when using the proposed KL-constrained reweighting scheme using 5 dual steps.



Table 12: Samples from models fine-tuned using multiple rewards with equal weights and with our constrained alignment method.



Table 13: Images sampled from models finetuned to maximize MPS [58], along with sharpness and saturation penalizations. We compare optimizing an equally weighted objective against our constrained approach.